Strike-slip tectonics in the SW Barents Sea during North Atlantic rifting [Swaen Graben, Northern Norway]

Omosanya, K.O.[a], Zervas, I[a]., Mattos, N.H[b], Alves, T.M[b], Johansen, S.E[a], George M[a]

[a] Department of Geoscience and Petroleum, Norwegian University of Science and Technology, 7491. Trondheim, Norway

[b]3D Seismic Lab, School of Earth and Ocean Sciences, Cardiff University, Main Building-Park Place, CF10 3AT Cardiff, United Kingdom

Corresponding author: kamaldeen.o.omosanya@ntnu.no

Abstract

This study uses high quality, three-dimensional [3-D] seismic data to investigate the occurrence of strike-slip faults in the Swaen Graben, SW Barents Sea. The Swaen Graben is divided into two principal sub-basins:- SSB1 and SSB2. The along-strike and along–dip displacement variations and scale relationships are analyzed for forty-two [42] faults. The displacement profiles for these faults are complex in the Swaen Graben, showing clear evidence for polycyclic fault growth and marked syn-sedimentary activity. The observed variations in the displacement profiles indicate complex along-strike segmentation, linkage and mechanical interactions at distinct structural levels. Along-dip displacement minima indicate fault reactivation by dip-linkage. Importantly, geometric evidence for strike-slip faulting in the Swaen graben includes the presence of extensional horsetail splay faults, positive flower structures and minor transfer faults. This study shows that the faults in the Swaen Graben developed under extensional regimes during Late Jurassic to Early Cretaceous rifting and were reactivated by regional stresses during the Late Cretaceous. The two principal strike-slip faults in the Swaen Graben reveal sinistral movement and are linked at a shallow depth by minor transfer faults at a relay zone. Our work further demonstrates the occurrence of Late Mesozoic strike-slip movements in the SW Barents Sea, which were induced by regional tectonics, halokinesis and fault block rotation. Importantly, strike-slip faulting in the region extends perhaps into the Cenozoic interacting with extension during the North Atlantic rifting.

Keywords: Swaen, Graben, Strike-slip, Displacement, Horsetail, Flower structures

This article has been accepted for publication and undergone full peer review but has not been through the copyediting, typesetting, pagination and proofreading process which may lead to differences between this version and the Version of Record. Please cite this article as doi: 10.1002/2017TC004635

1. Introduction

The tectonic evolution of the Swaen Graben and several other structural elements of the Barents Sea remains poorly understood mostly because of a general lack of stratigraphic control and high-quality data to constrain the structures and ages of several stratigraphic units in Northern Norway [*Gabrielsen, 1990; Omosanya et al., 2016*]. Previous work that described the geology of the Barents Sea chiefly relied on the interpretation of regional gravity, magnetic and two-dimensional [2-D] seismic lines [*Breivik et al., 1995, 1998; Faleide et al., 1993a; Gabrielsen et al., 1990; Gabrielsen, 1984; Gernigon and Brönner, 2012; Gudlaugsson et al., 1998*]. These previous works suggested that the Barents Sea developed into a mosaic of basins, structural highs and platforms from the Paleozoic to the present through the interplay of complex episodes of orogenies and extensional pulses [*Doré et al., 1999; Faleide et al., 1984; Henriksen et al., 2011; Smelror et al., 2009; Barrère et al., 2009*]. The evolution of the Barents Sea is the product of the complex interaction of large-scale processes that were controlled by plate tectonics, changing climate, and depositional conditions over several million years [*Doré, 1995; Faleide et al., 1984, 1993; Henriksen et al., 2011; Smelror et al., 2009; Barrère et al., 2009; Omosanya et al., 2015; Mattos et al., 2016*]. Hence, several basins, structural highs, and platforms formed in the Barents Sea at different stages during the Late Paleozoic and Mesozoic [*Doré, 1991; Gabrielsen, 1984; Nøttvedt et al., 1993; Ritzmann and Faleide, 2007*].

At a regional scale, the evolution of the Swaen Graben remains a subject of debate. This basin was first described as an extensional feature that originated during a major tectonic episode that affected the North Atlantic and Barents Sea regions during the Late Jurassic [e.g., *Svånå 2013*]. In this model, the Swaen Graben developed alongside the Asterias Fault Complex, the Eastern Flexure and the Loppa High [*Gabrielsen et al., 1990*]. In a further investigation of the Southwest Barents Sea, *Gabrielsen et al.* [2011] highlighted the effect of strike-slip movement on the continental margin where the Swaen Graben is located. However, until the present, strike-slip movements along the eastern section of the Loppa High remained unclear within the regional 2-D seismic record. Instead, strike-slip that was related to tectonic inversion was recognized to the west and south of the Loppa High and was dated as Late Paleozoic, Mesozoic and Cenozoic [*Gabrielsen et al., 2011; Safronova et al., 2014*]. The oldest documented strike-slip events in the study area were interpreted to be right-lateral movements that were related to the post-Caledonian structuring of the Barents Sea [*Faleide et al., 1984; Gabrielsen et al., 2011*]. A positive flower-like structure was observed in the Aptian–Hauterivian strata along the western segment of the Asterias Fault Complex. The youngest strike-slip events in the Barents Sea were related to the opening of the Norwegian-Greenland Seas and the development of the De Geer Shear Zone [*Faleide et al., 1984*].

This study aims to elucidate the tectonic evolution of the Swaen Graben by evaluating its geometry and growth with conventional fault-analysis methods. We aim to address the following questions:

a) What fault types bound the Swaen Graben and are associated with their formation?
b) Is it possible to investigate the history of fault growth and propagation in the Swaen Graben by using conventional displacement analysis tools?
c) Did the faults in the Swaen Graben entirely form under an extensional regime? Did late stage strike-slip movements affect the faults in the study area?
d) Assuming the occurrence of strike-slip faults in the Swaen Graben, when did they form and what is their importance to the regional tectonics of the SW Barents Sea?

To address these questions, we use displacement data to infer the fault-growth geometries [e.g., *Muraoka and Kamata, 1983; Nicol et al., 1996; Cartwright and Mansfield, 1998; Ferrill and Morris, 2001; Xu et al., 2010*]. Displacement plots are applied to investigate fault nucleation, propagation, segmentation and linkage in the study area [*e.g., Cartwright and Mansfield 1998; Baudon and Cartwright, 2008; Walsh and Watterson, 1987; Peacock and Sanderson, 1991; Mouslopoulou et al., 2007; Pochat et al., 2009; Thorsen, 1963; Omosanya and Alves, 2014; Omosanya et al., 2015; Mattos et al., 2016; Mohammedyasin et al., 2016*]. Importantly, we emphasize the role of the Swaen Graben as a key accommodation zone for displacement transfer between two adjacent sub-basins [SSB1 and SSB2], an observation of great relevance in the context of regional fault activity in the Barents Sea.

2. Geological setting

The Swaen Graben and all the surrounding structural elements are located on the Barents Sea Shelf [Figure 1]. The Barents Sea represents a large epicontinental sea in the northernmost Europe and covers an area of approximately 1.3 million km^2, with an average water depth of 300 m [*Faleide et al., 1984; Doré, 1995*]. In detail, the Swaen Graben is bounded by two opposing normal faults that roughly trend east-west [Figure 1]. The Loppa High and the Bjarmeland Platform bound the Swaen Graben to the west and east, respectively. The Norvag and Samson Domes are located to the north and south of the study area, respectively [Figure 1].

The Caledonian Orogeny dominated the tectonic evolution of the western Barents Sea at approximately 400 Ma [*Faleide et al., 1984; Gernigon et al., 2014; Johansen et al., 1994*]. The occurrence of the important NE-SW structural fabrics in the southwestern Barents Sea reflects the influence of the Caledonian Orogeny [*Doré, 1991; Johansen et al., 1994*], which deformed the crystalline basement of the western Barents Sea from the Late Silurian to the Early Devonian [*Faleide et al., 1984; Gudlaugsson et al., 1998*]. The proto-Atlantic extension in the west, opening of the Euramerican Basin to the north, transpression, transtension, and opening of the Norwegian-Greenland Sea in the Cenozoic [*Brekke and Riis, 1987; Doré, 1991, 1995; Breivik et al., 1998; Breivik et al., 2002; Dengo and Røssland, 2013; Worsley 2008*] later influenced the present-day tectonic configuration of the Barents Sea.

The oldest Paleozoic successions in the study area were deposited over a metamorphic basement that is dominated by Caledonian structures [*Doré, 1991 and Johansen et al., 1994*]. The oldest strata in the Barents Sea were deposited during the Svalbardian tectonic event, which involved phases of transtension and transpression during the Devonian, and in association with Carboniferous to Permian rifting [*Gabrielsen et al., 1990; Gudlaugsson et al., 1998*]. Continental rifting during the Late Paleozoic was synchronous with the collapse of the newly formed Caledonian Orogenic belt and the progressive break-up of the Pangea supercontinent [*Doré, 1995*]. Thus, the Paleozoic strata in the Barents Sea include carbonates, coal, evaporites and siliciclastic rocks because marine sedimentation prevailed during the Late Paleozoic [*Doré, 1995; Heafford, 1988; Gudlaugsson et al., 1998*]. During the Triassic, the entire SW Barents Sea was isolated from other Central European Basins [Doré, 1995], although high subsidence and sedimentation rates continued across the Barents shelf. By the Middle-Triassic, the entire Barents Shelf was under marine conditions [*Smelror et al., 2009 and Worsley, 2008*], with most of the southern to western shelf comprising an oscillating but generally northwest-prograding coastline. In such a setting, sand was at first sourced from the Baltic shield, and later increasingly from the Urals during the Early to Middle Triassic [*Worsley, 2008; Fleming et al., 2016*]. The Late Triassic was characterized by the extensive westward progradation of nearshore and coastal depositional environments. Prodelta shales dominated throughout most of the southwestern Barents Shelf during this period [*Smelror et al., 2009; Worsley, 2008*].

The northward propagation of the Atlantic rift system during the Middle Jurassic to Early Cretaceous created a marine connection across the western margin of the Barents Shelf [*Smelror et al., 2009*]. The Middle and Late Jurassic were dominated by regional extension in the SW Barents Sea. Relatively minor strike-slip fault systems also developed during the Jurassic [Gabrielsen et al., 1990]. Overall, the Mesozoic Era recorded regional subsidence with the formation of large interior sag basins throughout the Barents Sea [*Dore 1995; Glørstad-Clark et al., 2010*]. Marine sedimentation was ubiquitous and was dominated by the deposition of thick continental-shelf sequences that consisted of marine shales, siltstones, and sandstones [*Dalland et al., 1988 and Glørstad-Clark et al., 2010*]. Differential loading during this period triggered tectonic tilting and salt diapirism [*Gernigon et al., 2014, Mørk et al., 1999 and Worsley, 2008*]. In addition, the uplift of the Northern Barents Sea during the Early Cretaceous was associated with a major volcanic episode along the Kong Karls Land, Franz Josef Land and adjacent offshore areas [Worsley, 2008] [Figure 1]. This magmatic event was contemporaneous with the inception of continental break-up and opening of the Arctic Ocean [*Smelror et al., 2009*].

During the Late Cretaceous, rifting in the North Atlantic led to the reactivation of normal faults along the western margin of the Barents Sea, which was accompanied by local compression and uplift on the Svalbard Platform [Faleide et al., 1984, 1993; Gabrielsen et al., 1990]. Successive rifting episodes during the Cretaceous thus led to rapid subsidence and the development of major deep-water basins such as the Harstad, Tromsø, Bjørnøya and Sørvestsnaget basins [*Faleide et al., 1993*]. The Late Cenozoic development of the Barents Sea shelf was dominated by extensive regional uplift

and erosion [*Faleide et al., 1984; Knutsen and Larsen, 1997*]. The erosion and re-deposition of sediment are thought to have been particularly intense during the Pleistocene glaciations [*Øvrebø and Talleraas, 1977; Doré, 1995; Omosanya et al., 2016; Mattos et al., 2016*].

3. Data and methods

The data that were used for this study include two-dimensional [2-D] and new three-dimensional [3-D] seismic reflection data alongside four industry wells. The new 3-D seismic data cover an area of approximately 1,840 km^2 on the Bjarmeland Platform and Swaen Graben [Figure 1]. The inline and crossline spacing for the seismic cube was ~19 m and ~12.5 m, respectively, and the recording lengths and vertical sampling rates were 4500 ms and 4 ms, respectively. With a dominant frequency of 40 Hz and an average velocity of 2500 m/s as estimated from the borehole data, the vertical and horizontal resolutions were ~15.6 m and ~12.5 m, respectively. Furthermore, two 2-D lines were used to locate the study area in the context of the Barents Sea's regional geology [Figures 1 and 2]. All the seismic sections were displayed by using the normal American Society of Exploration Geophysicists [SEG] convention for a zero-phase wavelet. An increase in acoustic impedance with depth is a peak or a positive reflection, which are represented as black reflection on seismic sections. Relative decreases in acoustic impedance with depth are shown as negative or red reflections. A regional correlation panel was compiled across four [4] wells in Figure 3 to define lithology and ages of the interpreted horizons. The analyzed wells included 7225/3-1, 7224/6-1, 7224/7-1 and 7125/4-1.

The seismic interpretation included horizon and fault mapping, fault-displacement analysis, and seismic-attribute analysis. Nine surfaces that were tied to formation tops in the available wells were interpreted across the entire cube. Apart from the seabed, the eight horizons were named H1 to H8 [Figures 3 to 9]. Based on these horizons, the study area was further divided into seven main stratigraphic units, which range in age from Carboniferous to Cenozoic. The seismic attribute "variance" was used as an initial tool for fault identification and mapping. Variance is the direct measurement of the dissimilarity of seismic traces. Variance maps convert a volume of continuity into a volume of discontinuity, highlighting structural and stratigraphic boundaries [*Brown, 2004*]. On variance attribute maps, faults represent trace-to-trace variability and are mapped as high variance coefficient features.

Fault propagation and evolution were assessed by using fault-displacement analyses. The displacement plots that were used for this purpose included the maximum displacement [D_{max}] versus fault length [L] to understand the fault scaling relationship. Displacement-depth plots [D-z] were used to assess fault initiation, interaction, reactivation by dip-linkage and modes of fault propagation in cross section. Displacement-distance plots [D-x] were used to understand fault growth, segmentation and linkage along strike view. Fault throw was measured as the vertical separation in milliseconds two-way travel time [ms TWTT] between the footwall and hanging wall cut-offs of an interpreted horizon, in seismic sections that were perpendicular to the fault strike. The maximum errors of the throw measurements were estimated to be fixed and equivalent to the vertical sampling interval of 4 ms TWTT. The sampling interval determined the accuracy when matching two correlative seismic reflection peaks or troughs, not the vertical stratigraphic resolution, as is sometimes assumed [*see comments in Baudon and Cartwright, 2008; Ze and Alves, 2017*]. When the horizons are easily tied across faults, the correlation error in the throw measurement is eliminated. The errors of the fault drag were eliminated by excluding the trim area from the fault cut-off points [*see Whipp et al., 2014; Wilson et al., 2013*].

4. Results

4.1 Interpreted horizons and seismic units

The horizons that define the principal units in this work are shown from Figures 2 to 9. Horizons H1 to H3 were not penetrated by well 7224/6-1 and thus, were interpreted based on their amplitude characteristics. Their ages were established based on the regional geology. Horizon H1 is a component of the Ørn to Isbjørn Formations, i.e., the top of the regional carbonate platform and build-ups in the Barents Sea [*Larssen et al., 2002; Glørstad-Clark et al., 2010; Alves, 2016*]. The regional stratigraphic correlations that were published in *Mattos et al.* [2016] suggested that H2 and H3 represent the tops of the Early Triassic Havert and Klappmyss Formations. Horizons H4 to H8 correspond to the tops of the Middle Triassic Kobe, Late Triassic Snadd, Upper Jurassic Fuglen, Lower Cretaceous Knurr and Upper Cretaceous Kolmule Formations in well 7224/6-1, while the sea floor [horizon SBD] corresponds to the top of the Nordland Group [Figures 3 and 4]. Based on the ages of the interpreted horizons, the stratigraphy of the study area was divided into seven principal units that range from Carboniferous to Cenozoic in age [Figure 2].

The oldest unit in the study area is Unit 1, which is delimited by H1 to H2. The upper portion of Unit 1 shows low- to high-amplitude continuous seismic reflections, whereas its lower portion shows high-amplitude wavy and mounded reflections, which are interpreted to be carbonate build-ups. Hence, the lowermost unit in the study area is interpreted as part of the Carboniferous Falk to Ørn Formations [Figure 3 and 4]. Based on the regional correlations, the top of Unit 2 and the base of Unit 3 are either Early Triassic or Late Permian in age. Unit 3 comprises medium- to high-amplitude continuous seismic reflections [Figure 2]. Horizon H3 marks the top of Unit 3 and is represented by the Snadd Formation, which consists of thick shales that laterally change into interbedded shales, siltstones and limestones and carbonate-cemented sandstones that were deposited from the Ladinian to the Early Norian [*Dalland et al., 1988*]. Well 7224/6-1 does not penetrate the entire unit and, so, the lithology and age of its basal strata could not be precisely determined.

Unit 4 corresponds to the interval within horizons H6 and H5. Horizon H6 corresponds to the top of the Fuglen Formation, which consists of mudstones with interbedded thin limestones and was deposited during a marine highstand that was contemporaneous with tectonic activity from the Callovian to Oxfordian [*Deegan and Scull, 1977, Dalland et al., 1988*]. Horizon H5 is the base of Unit 4 and corresponds to the top of the Late Triassic Snadd Formation. Unit 5 is delimited by H7 and H6 at their top and base, respectively [Figures 2 to 9]. Horizon H7 marks the top of the Early Cretaceous Knurr Formation and H6 marks the top of the Late Jurassic Fuglen Formation [Figures 3 and 4]. These two stratigraphic markers comprise high-amplitude continuous seismic reflections, which are faulted in the Swaen Graben. The Knurr Formation comprises grayish-brown claystones that are interbedded with limestone and dolomite, all of which were deposited in an open and distal marine environment from the Ryazanian/Valanginian to Early Barremian. The top of Unit 6 marks the Late Cretaceous unconformity, i.e. the top of the Kolmule Formation [*Mattos et al., 2016*]. The Kolmule Formation consists of dark gray shales that are interbedded with sparse intervals of siltstone and sandstone and were deposited in an open marine environment from the Aptian to Middle-Cenomanian [*Dalland et al., 1988; Deegan and Scull, 1977; Omosanya et al., 2015*].

Unit 6 is marked at its top by a high-amplitude continuous reflection. This unit is very distinct because it predominantly consists of low amplitude reflections between high amplitude reflection layers [Figures 7 to 9]. On the seismic profiles, the youngest unit is Unit 7, which is marked by low- to medium-amplitude continuous reflections [Figures 7 to 9]. The top of Unit 7 is the present-day seabed [SBD], while H1 [Top Kolmule] is the base of this unit [Figures 2, 7 to 9]. Unit 7 consists of interbedded claystone, siltstone and sandstone that were deposited in bathyal to glacial marine environments from the Early Miocene to the present [*Deegan and Scull, 1977*].

4.2 Interpreted faults

The faults in the study area showed normal offsets on the seismic sections [Figures 7 to 9]. On the variance time-slices, the faults showed low variance coefficients [Figure 5a]. Hence, we could consistently follow and interpret the faults along the strike by combining the seismic sections and variance time slices. Structural maps that show the plan view geometry of the faults were generated by tracing the faults on the variance time slices [Figures 5b to 5d]. The forty-two faults that were interpreted in this work include those that offset the Permian to Early Cretaceous units i.e., Horizons H1 to H7. The fault orientations are NE-SW, NW-SE, WNW-ESE and NNW-SSE [Figure 6]. Most of the interpreted faults are clustered in the northern section of the study area, dividing the Swaen Graben into two sub-basins called SSB1 and SSB2 [Figure 5]. Fault F14 separates SSB2 from the Bjarmeland Platform, where fewer faults were interpreted [Figure 5].

The interpreted faults were further categorized into four fault types based on their perceived geometries on the seismic sections and TWTT structural maps. Type 1 faults were the longest faults that bounded sub-basins SSB1 and SSB2 in the study area [Figures 5b to 5d]. These faults are segmented laterally and possibly represent strike-slip faults. Examples of Type 1 faults include F5, F14, and F18 [Figures 7b and 8b-d]. Type 2 faults were initially likened to pop-up structures, which are common for restraining bends along strike-slip faults. At the Early Cretaceous level, strata that were associated with this fault type appeared to be shortened, with the H6 to H7 strata mildly uplifted relative to the underlying Triassic intervals [Figures 7b and 8b-d]. Type 2 faults are common along the southern margin of SSB1, e.g., F10, F16, and F26. The Type 3 faults on the seismic sections were synthetic with a general NE dip direction, suggesting that these faults comprise Riedel shears that formed at angles from 20^0 to 30^0 to F16 and F18. These Type 3 faults include F21 and F23. The upper tips of the Type 3 faults are truncated by H7, while the lower tips are limited to the Triassic

strata [Figures 8d and 9b]. Type 4 faults, including F33 and F37 [Figure 9], are found on the Bjarmeland platform, usually with their upper tips truncated by H6, i.e., the base of the Early Cretaceous strata [Figure 2]. These faults that do not extend above H6 and can be described as isolated beyond H2 because they show no interaction with other faults in map view [Figure 5]. Additionally, these faults are geometrically decoupled because their propagation is restricted to the H2-H6 strata [Figure 9].

4.3 Fault-displacement analyses

Maximum displacement [D_{max}] vs. fault length plots were used to understand how the fault geometry varied over different length scales for the forty-two faults [Figure 10]. The D_{max} vs. Length [L] plots were estimated from horizons H2 to H7. The majority of the interpreted faults had a D/L ratio between 1:100 and 1:1000. The coefficients of correlation 'R' between the maximum displacement and fault length ranged from 0.35 to 0.52. R2, which is the coefficient of determination for the faults, ranged from 0.13 to 0.27. The values of the exponent for the power law ranged from 0.50 to 0.87 [Figure 10]. Furthermore, representative faults among each of the fault types were used for the D-x plots. In Figure 11, the plots are shown from H2 to H7. While single and isolated faults are depicted on D-x profiles as a nearly symmetric slope, faults with abrupt displacement variations indicate the linkage of individual segments through the displacement minima [Muraoka and Kamata, 1983; Walsh et al. 2003].Type 1 faults such as F14 had very complicated D-x profiles. For H6 and H7, the profiles were skewed C-type profiles, combining into three to four segments with maximum displacements of approximately 140 m. In contrast, more segments than those of the shallower horizons characterized the profiles for F14 from H2 to H5. The individual segments had similar D-x profiles to C-type profiles of Muraoka and Kamata [1983]. However, the profiles were M-types at the fault tips, changing F14 into a skewed C-M profile from H5 to H2 [Figure 11a]. Furthermore, the direction of the skewness for the profiles changed from the top to the bottom horizons and from one tip to the other [Figure 11a]. Conversely, the Type 2 faults had more segments than the Type 1 faults. Each segment displayed C-type profiles except on H6, where the profile for F10 was skewed.

The maximum displacement across the interpreted horizons reached 450 m [Figure 11b]. The D-x plots for the Type 3 faults were only estimated on H6 and H7 [Figure 11c]. The plots showed simple profiles including C-type and skewed C-type profiles. For the Type 4 faults [e.g., F33], the D-x plots had much simpler profiles, being less segmented relative to the other fault types and generally characterized by both C- and M-type profiles [Figure 11d]. Thus, faults with simple D-x plots thus were less segmented along their strike. The maximum displacement on H6 and H7 may coincide with the point of fault nucleation. H6 to H7 delimits the Early Cretaceous strata and thus probably indicates the timing of fault nucleation.

The Displacement [D]-depth [z] plots for all the faults along their strikes provide a simple to complex history of fault nucleation and propagation. For all the plots, the position of D_{max} varied from H6 to H3 and H2 [Figure 12]. The majority of the faults had their d_{max} at H6 signifying that most of the faults probably nucleated during the Early Cretaceous [Figure 12]. The Type 1 faults had the most complicated profiles, showing marked variations in the D-z plot along with strike variation. At the two tips of the faults, F14 had hybrid profiles that consisted of two segments [Figure 12]. For the Type 2 faults [F10], the central position was characterised by upwardly skewed C-type profiles, in contrast to the M-type profiles at the tips. On the other hand, the Type 3 faults had simple M-type profiles, with the position of d_{max} restricted to H6 [Figure 12]. Here, the maximum displacement reached 40 m. Although the D-z profiles were mostly M-type profiles, we could consider some of them as skewed M-type profiles. Furthermore, the Type 4 [F33] faults generally showed an upward increase in displacement and were skewed towards d_{max} [Figure 12].

5. Discussion

5.1 Geometry and growth history of the faults within the Swaen Graben

The scale relationships of faults within the Swaen Graben were first compared to values from previous studies [*e.g., Muraoka and Kamata, 1983; Walsh and Watterson, 1987; Peacock and Sanderson, 1991; Dawers et al., 1993; Schlische et al., 1996*]. The general relationship between the maximum displacement [D_{max}] and fault length [L] was assumed to be $D_{max}=cL^n$, where the exponent value, "n", can range from 0.5 to 2.0 [*Walsh and Watterson, 1988; Gillespie et al., 1992; Cowie and Scholz, 1992; Dawers et al., 1993; Schlische et al., 1996; Fossen and Hesthammer, 1997*]. Self-

similar faults usually have an exponential value of n=1 while faults with scale-dependent geometry are generally characterized by n value that is not equal to one [*Kim and Sanderson, 2005*]. The value of c is an expression of fault displacement over a unit length. For a linear scaling, c is simply the ratio d_{max} /L when n=1 [*Kim and Sanderson, 2005*]. The constant c mainly depends on the rock properties [Walsh and Watterson, 1987; Mansfield and Cartwright, 1996]. The values of the parameters for the fault-scaling relationships have been investigated on normal, thrust and strike–slip faults. For example, thrust faults have slightly higher values from 0.02 to 0.1 [*Kim and Sanderson, 2005*]. This fault-scaling law implies that isolated faults that transect a rock with uniform properties i.e., with a constant value of c should retain a constant D/L ratio as they grow [*Cowie and Scholz, 1992 and Dawers et al., 1993*]. The D_{max} versus L for the faults in the Swaen Graben showed exponential values from 0.5 to 0.87, which are similar to previously reported values in several other tectonic settings. Similarly, the D/L values of 10^{-2} match those of geological faults around the Earth [10^{-2} to 10^{-3}]. The rock properties, types of faults, slip/propagation histories, segmentation and linkage, and reactivation are some of the factors that control the D_{max}/L ratio. Here, the marked variations in the value of n are attributed to the complex of evolution of the faults *vis-à-vis* fault segmentation and linkage.

The D-x and D-z plots implied the complex lateral and vertical segmentation of the faults. The history of fault growth in terms of nucleation, propagation, segmentation, linkage and reactivation was assessed from these two plots. The D-z plots in Figure 11 shows that the faults within the Swaen Graben can be classified into [a] those with simple growth histories [e.g., Types 3 and 4] and [b] those with polycyclic histories [Types 1 and 2]. In terms of fault nucleation, the Types 1 to 3 faults had their d_{max} on H6, which could be the point of fault nucleation if the effect or influence of fault segmentation and mechanical heterogeneity was neglected. The position of d_{max} can migrate from the fault-nucleation site because of interaction with other faults or the presence of mechanical barriers [*e.g. Cowie, 1998; Peacock, 1991; Schultz, 2000; Omosanya and Alves, 2014; Omosanya et al., 2015, 2016*]. In contrast, the Type 1 faults had variable points for $d_{max,}$ i.e., from H2 to H6 signifying their complex history of nucleation and interaction. The preponderance of d_{max} within the H6-H7 strata therefore implies an Early Cretaceous age for fault growth, which coincides with Cretaceous rifting in the Barents Sea [Figure 3]. This hypothesis is further supported by the burial of most all the interpreted faults by the Late Cretaceous strata. Additionally, the syn-kinematic strata interpreted from H5 to H6 suggested that some of the faults could have nucleated during the Late Jurassic.

Apart from fault nucleation, the geometry of the D-z plots offers insight into the fault-propagation history through either isolated or coherent models [Tvedt et al., 2013]. Although, the use of throw profiles to characterize fault propagation histories requires significant assumptions because faults can transition between blind and syn-sedimentary activity [*Childs et al., 1993; Meyer et al., 2002; Nicol et al., 1996*]. Nonetheless, the D-z plots for the Type 4 faults showed a distinct upward increase in displacement with depth, signaling propagation through syn-sedimentary activity. This phenomenon was also true for some sections of the Type 1 to 3 faults. Only the lower segments of the Type 1 and 4 faults showed radial or blind propagation [Figure 12]. The upward increase in displacement indicates syn-sedimentary activity, while the faults with centralized d_{max} indicate the radial fault propagation of the fault tips [*Omosanya and Alves, 2014; Omosanya et al., 2015; Mohammedyasin et al., 2016*]. The combination of both blind and syn-sedimentary activity on a single fault thus indicates a polycyclic history. Additionally, the dominant the M-type profile of Type 3 faults signifies frictional resistance to fault growth at the tips [*Muraoka and Kamata, 1983*]. Evidence for the reactivation of faults is indicated by displacement minima [D_{min}] on F14 [Figure 12]. Reactivation occurred through dip-linkage, which occurs when initially isolated fault sets coalesce into a single coherent structure by accumulating displacement over time. Dip-linkage is marked on D-z profiles by displacement minima that connect discrete segments of a fault [cf. *Mansfield and Cartwright, 1996; Omosanya and Alves, 2014; Mohammedyasin et al., 2016*].

Lateral fault linkage and segmentation were more complicated than those along the dip [Figures 5 and 11]. The D-x plots varied from simple to complex. For example, the Type 1 and 4 faults had fewer segments than the Type 2 faults. The D-x plots were also characterized by multiple positions for d_{max} from H2 to H7. Individual segments on the D-x plots had centralized d_{max} position or C-type profiles, indicating radial propagation. In contrast, the M-type profiles were located at the farthest tips of the Type 4 faults [Figure 11]. C-type faults are characteristic of homogeneous incompetent materials, whereas M-types are representative of faults that cut through a rigid unit [Muraoka and Kamata, 1983]. Astonishingly, the location of d_{max} for Type 1 faults varied from deeper

stratigraphic levels to shallower ones, producing three distinct segments with different d_{max} from left to right. The d_{max} position was to the right from H7 to H6, at the center for H5 and to the left for H2-H4 [Figure 11]. This variation or anisotropy in skewness [a] also indicates the complex evolution of the faults and [b] suggests that the faults coalesced in both the vertical and lateral directions, signifying oblique slip along the fault plane.

5.2 Geometric evidence for strike-slip movement in the Swaen Graben

Three distinctive structures were analyzed to provide evidence for strike-slip movement within the Swaen Graben. These structures include [a] kinematic indicators of strike-slip faults, such as the horsetail sigmoidal geometry from F21 to F24, e.g., *Dooley and Schreurs*, [2012] and *Schreurs* [2003] [b] flower or pop-up structure in F11, F12 and F14; and [c] relay zones between the sub-basins SSB1 and SSB2, from F18 to F14. The first evidence for strike-slip faulting in the Swaen Graben is the sigmoidal horsetail geometry of splay faults that are associated with F18 [Type 1 fault] in map view. These faults are generally oriented NE-SW, curving away from F18 like an imbricate fan, and formed on the footwall of F18 [Figures 5 and 13]. Horsetail faults are second-order faults that initiate at the around-tip damaged zone in plain view and are mainly observed in strike-slip systems [*McGrath and Davidson, 1995; Kim et al., 2004; 2003; Mouslopoulou et al. 2007; Zampieri and Massironi, 2007; Choi et al. 2016*]. Damage zones are classified into three major categories; along-fault or -wall damage zone, around-tip or tip damage zones and linked damaged zone [*Fossen et al., 2005; Childs et al., 2009; Choi et al., 2016*]. As second-order faults, horsetail splays form from fault-tip propagation through the sediments. Their fault traces can be parallel to strike-slip components [Mode II tip] and/or perpendicular to dip-slip components [Mode III tip] in relation to the main slip sense [*Atkinson, 1989; McGrath and Davidson, 1994; Kim et al., 2004; 2003; Dooley and Schreurs 2012; Choi et al. 2016*]. The sigmoidal shape of the horsetail faults developed because of variations in the displacement sense or block rotations between the master faults and thus can be used as kinematic indicators for strike-slip movement [*Kim et al., 2003; Dooley and Schreurs, 2012*]. Horsetail splay faults can form within either the footwall or hanging-wall of major faults, revealing the direction of fault propagation in cross sections. The horsetail geometry signifies downward propagation when these features form within the footwall and upward propagation when they form within the hanging wall [*McGrath and Davidson, 1995; Friedman and Logan, 1970*]. Hence, the horsetail geometry on the footwall of F18 indicates downward fault propagation and strike-slip movements for faults F19-F24 [Figures 13 and 14]. However, the 'lazy' S shape of the horsetail structure indicates oblique slip motion with sinistral transtensional components for F18 and the other Type 3 faults [Figures 13 and 14]. Therefore, these Type 3 faults are second-order faults with mixed modes of II and III fault propagation.

The second evidence for strike-slip faulting in the study area is the presence of pop-up structures within the hanging wall of F14 [Figures 14 to 16]. The splay faults that are associated with F14 include F11 and F12 and are marked as uplifted block that create positive flower structures in the seismic sections [Figures 15a and 15b]. We systematically mapped these pop-up structures by using the time slices from 980 ms to 1152 ms to interpret several small faults that are oriented to the NE-SW. The interpreted flower structure showed a relief that decreased toward the southern section of F14, resembling a fan-like geometry in the seismic sections [Figure 15]. Additionally, the H6-H7 strata showed variable thickness on both sides of F14 from north to south. F14 was interpreted as a transpressive strike-slip fault based on its nearly vertical geometry in Figure 15b, the opposite sense of displacement for the splay faults in its upper sections and the associated pop-up structure. Alternatively, the interpreted pop-up structures might actually be extensional faults with oblique-slip or evidence for mild-inversion at the upper section of F14. However, we stick to interpretation of this feature as a pop-up structure because of the uplifted H6-H7 strata and the monocline within the strata between H7 and H8 [Figures 15a and 15b].

The two principal sub-basins that were identified within the Swaen Graben are disparate units in map view at shallow depths. We mapped the geometry of the boundary faults by using the maps and discovered that the sub-basins SSB1 and SSB2 merged at depths from approximately 970 TWTT ms to 1820 TWTT ms [Figures 13 to 16]. This geometric relationship provides evidence for a relay zone between F18 [SSB1] and F14 [SSB2], which presumably transferred displacement across the two sub-basins. Walsh et al. [1999] defined a relay zone as the rock volume between kinematically related fault segments. Here, a relay zone was interpreted at the center part of the Swaen Graben, where F14 overlaps with F18 [Figures 13 and 16]. Relay zones are the products of several segments of extensional structures that interact and develop at the overlapping zone of two normal faults in a rift system [*Acocella et al. 2005; Peacock et al., 2000; Giba et al., 2012*]. As the displacement in the relay

zone increases, the strain in the transfer zone increases until it reaches a critical value, where the relay zone is eventually breached by normal faults [*Soliva and Benedicto, 2004; Childs et al., 2009; Giba et al., 2012; Morley et al., 1990*]. Variations in displacement within the overlapping zone can form high-angle transfer faults with strike-slip components [*McClay and White, 1995*]. In the study area, several minor or subfaults were identified in the relay zone [Figure 16b] and are therefore interpreted as transfer or strike-slip faults that developed between F14 and F18.

A conceptual model for the evolution of the faults within the Swaen Graben is presented in Figure 17. The sub-basins SSB1 and SSB2 within the Swaen Graben were delimited by strike-slip faults along their boundaries. At the boundary between sub-basins SSB1 and SSB2 was F18, which is a left-lateral transtensional fault associated with extensional horsetail splay faults while F14 is a sinistral transpressional faults that bounds sub-basin SSB2 and the Bjarmeland Platform. These two sub-basins are linked by transfer faults at the relay zone signifying that the faults in the Swaen Graben developed as extensional faults that were reactivated at the boundaries as strike-slip faults. The pop-up structures in Figures 14 and 15 provide evidence for the uplift of the H7-H8 strata and Late Cretaceous uplift because of lateral movements. Evidence for Late Cretaceous faulting is also shown through the Type 4 faults, which are buried beneath the H6-H8 strata. The preponderance of d_{max} positions at the H6 level and the syn-sedimentary activity that is shown by the majority of the faults signify that most of the faults initiated during the Late Jurassic to Early Cretaceous. Hence, extensional tectonics dominated the study area during the Late Jurassic to Early Cretaceous, corresponding to a regional rifting event in the Barents Sea during this time [*cf. Faleide et al., 1993a, 1993b*]. Strike-slip or lateral movement in the Swaen Graben was here dated to the Late Cretaceous and perhaps extends to the Early Paleogene. First, as a corollary of the overall structuring of the Hammerfest Basin and Asterias Fault Complex by extensional deformational style and strike-slip reactivation in Late Jurassic to Early Cretaceous [*Sund et al., 1986, Gabrielsen and Færseth 1989, Gabrielsen et al., 1990*]. *Berglund et al*. [1986] identified compressional strike-slip faults and flower structures in the Asterias Fault Complex. The strike-slip faulting in these locations and, by proxy, the Swaen Graben is associated with gravity-induced movements and the rotation of regional fault blocks around a vertical or horizontal axis [*Moretti et al., 1988; Ziegler et al., 1986; Gabrielsen and Færseth 1988, Gabrielsen et al., 1990*]. The gravity-induced transverse movement of the Hammerfest Basin towards the Tromsø Basin during the Late Cretaceous and the Early Cenozoic reactivated the faults in the Asterias and Troms-Finnmark Fault Complexes. During this movement, strike-slip movements were recorded along the southern Loppa High and Bjørnøyrenna Fault Complex [*Ziegler et al. 1986; Berglund et al., 1986; Gabrielsen and Færseth, 1988*]. In addition, salt halokinesis in the Svalis Dome, Tromsø Basin, Samson Dome, and Hammerfest Basin may have been added mechanisms that caused the strike-slip faulting in the Swaen Graben. Salt diapirism in the Tromsø Basin occurred probably during the Late Cretaceous to Late Cenozoic [*Spencer, 1984; Nilsen et al., 1995*] while Late Cretaceous to Early Paleogene salt-movement was recorded in the Samson Dome [*Breivik et al., 1995; Mattos et al., 2016*]. We propose that far-field stresses due to halokinesis could cause extensional faults in the Swaen Graben to reactivate in a lateral movement at the boundary of the SSB1 and SSB2. Hence, regional stresses that were coeval with the rotation of the Hammerfest Basin to the west and halokinesis in surrounding basins presumably caused the extensional boundary faults of the Swaen Graben to reactivate in strike-slip mode during the Late Cretaceous. We have no evidence for Early Paleogene faulting in the study area. Nonetheless, Early Paleogene strike-slip faulting could have been recorded in adjacent basins. Importantly, these transpressive and transtensive movements represent localized tectonic aberration that occurred prior and intermittently with the North Atlantic rifting.

6.0 Conclusions

This paper investigated the growth and types of faults within the Swaen Graben by using high-resolution three-dimensional [3-D] seismic reflection data and four wells. The main conclusions from this work are summarized as follows:

- Seismic interpretation facilitated the mapping of forty-two faults in the study area, which were further categorized into four fault types based on their geometries along seismic sections and maps. Based on the spatial distribution or fault clusters, the Swaen graben could be categorized into a southern sub-basin [SSB1] and a northern sub-basin [SSB2].
- Displacement plots showed that the interpreted faults have complex along-strike and along-dip profiles, which reflect their complex evolution, interaction, segmentation and linkage. Two

major episodes of faulting were identified based on the displacement plots and fault interactions with the Cretaceous sediments.

- During the first episode of faulting, the majority of the faults in the Swaen Graben nucleated at the Jurassic and Early Cretaceous interval and propagated through syn-kinematic activity concomitantly with Jurassic to Early Cretaceous rifting. A second phase of faulting include strike-slip movements, which started in Late Cretaceous and perhaps continued into Early Paleogene interacting with regional extension and North Atlantic rifting in Cenozoic. Strike-slip faulting during the second phase in the study area is tied to regional Mesozoic tectonics and halokinesis that affected most part of the SW Barents Sea in Late Cretaceous.
- In the Swaen Graben, the strike-slip faults are sinistral transpressional and transtensional faults in sub-basins SSB2 and SSB1. On the maps and seismic sections, strike-slip faults in SSB1 is geometrically revealed by extensional horsetail splay faults that were associated with its eastern margin whereas a positive flower structure is observed on the eastern boundary of SSB2. A third and minor class of strike faults are subfaults or transfer faults at the relay zone between SSB2 and SSB1, which linked the two sub-basins since the Late Cretaceous.
- Faults in the Swaen Graben are large boundary faults [Type 1] faults, which occasionally have extensional horsetail splay faults [i.e. Type 3] at their tips. Type 2 faults, which are the syn-sedimentary normal faults, that show boundary restrictions to fault growth at their tips and Type 4 normal faults.

Acknowledgements

This work was sponsored by the ARCEx project [Research Centre for Arctic Petroleum Exploration] which is funded by the Research Council of Norway [grant number 228107] together with 10 academic and 9 industry partners. We also acknowledge the Norwegian Petroleum Directorate [NPD] for graciously granting access to the borehole data used in this research [www.npd.no] and Schlumberger for provision of Petrel® and Petrel ready project for seismic interpretation. The seismic data for this work is part of the NTNU-Schlumberger Petrel-ready database and can be accessed at the Department of Geoscience and Petroleum, Norwegian University of Science and Technology, Trondheim [www.ntnu.no/igp]. Detailed information about the geology of the area and Lithostratigraphy of the boreholes can be found at website of the Norwegian Petroleum Directorate [www.npd.no]. We thank Tony Doré and an anonymous reviewer for their outstanding and constructive reviews. We are also grateful to the editor and the associate editor for their contributions during the review process.

References

Acocella, V., Morvillo, P., and Funiciello, R. [2005]. What controls relay ramps and transfer faults within rift zones? Insights from analogue models. *Journal of Structural Geology*, *27*[3], 397-408.

Alves, T.M., [2016]. Polygonal mounds in the Barents Sea reveal sustained organic productivity towards the P–T boundary. Terra Nova 28, 50–59. doi:10.1111/ter.12190

Atkinson, B. K. [Ed.]. [1989]. *Fracture mechanics of rock*. Academic Press. London.

Barrère, C., Ebbing, J. and Gernigon, L. [2009]. Offshore prolongation of Caledonian structures and basement characterization in the western Barents Sea from geophysical modelling. Tectonophysics, 470, 71–88.

Baudon, C., Cartwright, J. [2008]. The kinematics of reactivation of normal faults using high resolution throw mapping. Journal of Structural Geology, 30[8], 1072-1084.

Berglund, L., T., Augustson, G., Færseth, R., Ramberg-Moe, H. [1986]: The evolution of the Hammerfest Basin. In: A. M. Spencer [ed.]: Habitat of Hydrocarbons on the Norwegian Continental Margin. Norwegian Petroleum Society [Graham and Trotman], pp. 319-338

Breivik, A. J., Faleide, J. I., and Gudlaugsson, S. T. [1998]. Southwestern Barents Sea margin: late Mesozoic sedimentary basins and crustal extension. *Tectonophysics*, *293*[1], 21-44.

Breivik, A. J., Gudlaugsson, S. T., and Faleide, J. I. [1995]. Ottar Basin, SW Barents Sea: a major Upper Palaeozoic rift basin containing large volumes of deeply buried salt. *Basin research*, *7*[4], 299-312.

Breivik, A. J., Mjelde, R., Grogan, P., Shimamura, H., Murai, Y., Nishimura, Y., and Kuwano, A. [2002]. A possible Caledonide arm through the Barents Sea imaged by OBS data. *Tectonophysics*, *355*[1], 67-97.

Brekke, H., and Riis, F. [1987]. Tectonics and basin evolution of the Norwegian shelf between 62 N and 72 N. *Norsk Geologisk Tidsskrift*, *67*, 295-322.

Brown, A.R., [2004]. Interpretation of three-dimensional seismic data. AAPG Memoir 42,, SEG Investigation in Geopysics.

Cartwright, J. A., and Mansfield, C. S. [1998]. Lateral displacement variation and lateral tip geometry of normal faults in the Canyonlands National Park, Utah. *Journal of Structural Geology*, *20*[1], 3-19.

Childs, C., Easton, S. J., Vendeville, B. C., Jackson, M. P. A., Lin, S. T., Walsh, J. J., and Watterson, J. [1993]. Kinematic analysis of faults in a physical model of growth faulting above a viscous salt analogue. *Tectonophysics*, *228*[3], 313-329.

Childs, C., Manzocchi, T., Walsh, J. J., Bonson, C. G., Nicol, A., and Schöpfer, M. P. [2009]. A geometric model of fault zone and fault rock thickness variations. *Journal of Structural Geology*, *31*[2], 117-127.

Choi, J. H., Edwards, P., Ko, K., and Kim, Y. S. [2016]. Definition and classification of fault damage zones: a review and a new methodological approach. *Earth-Science Reviews*, *152*, 70-87.

Cowie, P. A. [1998]. Normal Fault Growth in Three Dimensions in Continental and Oceanic Crust. *Faulting and magmatism at mid-ocean ridges*, 325-348.

Cowie, P. A., and Scholz, C. H. [1992]. Displacement-length scaling relationship for faults: data synthesis and discussion. *Journal of Structural Geology*, *14*[10], 1149-1156.

Dalland, A., Worsley, D., Ofstad, K. [eds.], [1988]: A lithostratigraphic scheme for the Mesozoic and Cenozoic succession offshore mid- and northern Norway. NPD-Bulletin No. 4, 65 pp.

Dawers, N. H., Anders, M. H., and Scholz, C. H. [1993]. Growth of normal faults: Displacement-length scaling. *Geology*, *21*[12], 1107-1110.

Deegan, C. E., and B. J. Scull, [1977]. A standard lithostratigraphic nomenclature from the central and northern North Sea: Institute of Geological Sciences Report, v. 77/25, 36 p

Dengo, C. A., and Røssland, K. G. [2013]. Extensional tectonic history of the western Barents Sea. *Structural and Tectonic Modelling and Its Application to Petroleum Geology, Norwegian Petroleum Society [NPF], Special Publication*, *1*, 91-108.

Dooley, T. P., and Schreurs, G. [2012]. Analogue modelling of intraplate strike-slip tectonics: A review and new experimental results. *Tectonophysics*, *574*, 1-71.

Doré A.G., Lundin, E.R., Jensen, L.N., Birkeland, *Ø*, Eliassen, P.E., and Fichler, C., [1999]. Principal tectonic events in the evolution of the northwest European Atlantic margin, *in* Fleet, A.J. and Boldy, S.A.R.,

Doré, A. G. [1991]. The structural foundation and evolution of Mesozoic seaways between Europe and the Arctic. *Palaeogeography, Palaeoclimatology, Palaeoecology*, *87*[1-4], 441-492.

Doré, A. G. [1995]. Barents Sea geology, petroleum resources and commercial potential. *Arctic*, 207-221.

Faleide, J. I., Gudlaugsson, S. T., and Jacquart, G. [1984]. Evolution of the western Barents Sea. *Marine and Petroleum Geology*, *1*[2], 123IN1129IN5137-128IN4136IN8150.

Faleide, J. I., Vågnes, E., and Gudlaugsson, S. T. [1993]. Late Mesozoic-Cenozoic evolution of the south-western Barents Sea in a regional rift-shear tectonic setting. *Marine and Petroleum Geology*, *10*[3], 186-214.

Ferrill, D. A., and Morris, A. P. [2001]. Displacement gradient and deformation in normal fault systems. *Journal of Structural Geology*, *23*[4], 619-638.

Fleming, E.J., Flowerdew, M.J., Smyth, H.R., Scott, R.A., Morton, A.C., Omma, J.E., Frei, D. and Whitehouse, M.J. [2016]. "Provenance of Triassic sandstones on the southwest Barents Shelf and the implication for sediment dispersal patterns in northwest Pangaea". Marine and Petroleum Geology 78: p516-535.

Fossen, H., and Hesthammer, J. [1997]. Geometric analysis and scaling relations of deformation bands in porous sandstone. *Journal of Structural Geology*, *19*[12], 1479-1493.

Fossen, H., Johansen, T.E.S., Rotevatn, A., and Hesthammer, J., [2005]. Fault interaction in porous sandstones. AAPG Bulletin 89, 1593e1606

Friedman, M., and Logan, J. M. [1970]. Microscopic feather fractures. *Geological Society of America Bulletin*, *81*[11], 3417-3420.

Gabrielsen, R. H. [1984]. Long-lived fault zones and their influence on the tectonic development of the southwestern Barents Sea. *Journal of the Geological Society*, *141*[4], 651-662.

Gabrielsen, R. H., Faerseth, R. B., and Jensen, L. N. [1990]. *Structural Elements of the Norwegian Continental Shelf. Pt. 1. The Barents Sea Region*. Norwegian Petroleum Directorate.

Gabrielsen, R. H., Faleide, J. I., Pascal. C., and Torsvik,T. H., [2011]. Plate tectonics and tectonic inversion in the Barents Sea, Abstract: AAPG 3P Arctic. The Polar Petroleum Potential Conference & Exhibition, 30 August – 2 September, Halifax, Nova Scotia, Canada, Search and Discovery Article # 90130

Gabrielsen, R., H., and Færseth, R., B., [1988]. Cretaceous and Tertiary reactivation of master fault zones of the Barents Sea [extended abstract]. In: W.K. Dallman, Y., Ohta and Andresen, A., [eds]: Tertiary Tectonics of Svalbard. Extended abstracts from Symposium held in Oslo 26 and 27 April 1988. Norsk Polarinstitutt, Report Series, p 46, 93-97.

Gabrielsen, R., H., and Færseth, R., B., [1989]. The inner shelf of North Cape, Norway and its implication for the Barents Shelf-Finnmark Caledonide boundary. A comment. Norsk geologisk tidsskrift, p 69, 57-62.

Gabrielsen, R., H., Færseth, R., B., Jensen, L., N., and Kalheim, J., E. [1990]. Structural elements of the Norwegian continental Shelf. NPD-Bulletin N 06, p. 12-15.

Gernigon, L., and Brönner, M. [2012]. Late Palaeozoic architecture and evolution of the southwestern Barents Sea: insights from a new generation of aeromagnetic data. *Journal of the Geological Society*, *169*[4], 449-459.

Gernigon, L., Brönner, M., Roberts, D., Olesen, O., Nasuti, A., and Yamasaki, T. [2014]. Crustal and basin evolution of the southwestern Barents Sea: from Caledonian orogeny to continental breakup. *Tectonics*, *33*[4], 347-373.

Giba, M., Walsh, J. J., and Nicol, A. [2012]. Segmentation and growth of an obliquely reactivated normal fault. *Journal of Structural Geology*, *39*, 253-267.

Gillespie, P. A., Walsh, J. T., and Watterson, J. [1992]. Limitations of dimension and displacement data from single faults and the consequences for data analysis and interpretation. *Journal of Structural Geology*, *14*[10], 1157-1172.

Glørstad-Clark, E., Faleide, J. I., Lundschien, B. A., and Nystuen, J. P. [2010]. Triassic seismic sequence stratigraphy and paleogeography of the western Barents Sea area. *Marine and Petroleum Geology*, *27*[7], 1448-1475.

Gudlaugsson, S. T., Faleide, J. I., Johansen, S. E., and Breivik, A. J. [1998]. Late Palaeozoic structural development of the south-western Barents Sea. *Marine and Petroleum Geology*, *15*[1], 73-102.

Heafford, A. P. [1988]. Carboniferous through Triassic stratigraphy of the Barents Shelf. *Geological Evolution of the Barents Shelf Region. Graham and Trotman, London*, 89-108.

Henriksen, E., Bjørnseth, H. M., Hals, T. K., Heide, T., Kiryukhina, T., Kløvjan, O. S., and Stoupakova, A. [2011]. Uplift and erosion of the greater Barents Sea: impact on prospectivity and petroleum systems. *Geological Society, London, Memoirs*, *35* [1], 271-281.

Indrevær, K., Gabrielsen, H., R., and Faleide, J.I. [2016]: Early Cretaceous syn-rift uplift and tectonic inversion in the Loppa High area, southwestern Barents Sea, Norwegian shelf. Accepted by Journal of the Geological Society of London. Doi: 10.1144/jgs2016-066.

Johansen, S. E., Henningsen, T., Rundhovde, E., Sæther, B. M., Fichler, C., and Rueslåtten, H. G. [1994]. Continuation of the Caledonides north of Norway: seismic reflectors within the basement beneath the southern Barents Sea. *Marine and Petroleum Geology*, *11*[2], 190-201.

Kim, Y. S., and Sanderson, D. J. [2005]. The relationship between displacement and length of faults: a review. *Earth-Science Reviews*, *68*[3], 317-334.

Kim, Y. S., Peacock, D. C. P., and Sanderson, D. J. [2003]. Mesoscale strike-slip faults and damage zones at Marsalforn, Gozo Island, Malta. *Journal of Structural Geology*, *25*[5], 793-812.

Kim, Y. S., Peacock, D. C., and Sanderson, D. J. [2004]. Fault damage zones. *Journal of structural geology*, *26*[3], 503-517.

Knutsen, S. M., and Larsen, K. I. [1997]. The Late Mesozoic and Cenozoic evolution of the Sørvestsnaget Basin: A tectonostratigraphic mirror for regional events along the Southwestern Barents Sea margin?. *Marine and petroleum geology*, *14*[1], 27-54.

Larssen, G. B., Elvebakk, G., Henriksen, L. B., Kristensen, S. E., Nilsson, I., Samuelsberg, T. J., and Worsley, D. [2002]. Upper Palaeozoic lithostratigraphy of the Southern Norwegian Barents Sea. *Norwegian Petroleum Directorate Bulletin*, *9*, 76.

Mansfield, C. S., and Cartwright, J. A. [1996]. High-resolution fault displacement mapping from three-dimensional seismic data: evidence for dip linkage during fault growth. *Journal of Structural Geology*, *18*[2-3], 249-263.

Mattos, N. H., Alves, T. M., and Omosanya, K. O. [2016]. Crestal fault geometries reveal late halokinesis and collapse of the Samson Dome, Northern Norway: Implications for petroleum systems in the Barents Sea. *Tectonophysics*, *690*, 76-96.

McClay, K. R., and White, M. J. [1995]. Analogue modelling of orthogonal and oblique rifting. *Marine and Petroleum Geology*, *12*[2], 137-151.

McGrath, A. G., and Davison, I. [1995]. Damage zone geometry around fault tips. *Journal of Structural Geology*, *17*[7], 1011-1024.

Meyer, V., Nicol, A., Childs, C., Walsh, J. J., and Watterson, J. [2002]. Progressive localisation of strain during the evolution of a normal fault population. *Journal of Structural Geology*, *24*[8], 1215-1231.

Mohammedyasin, S. M., Lippard, S. J., Omosanya, K. O., Johansen, S. E., and Harishidayat, D. [2016]. Deep-seated faults and hydrocarbon leakage in the Snøhvit Gas Field, Hammerfest Basin, Southwestern Barents Sea. *Marine and Petroleum Geology*, *77*, 160-178.

Moretti, I., Colletta, B., and Vially, R. [1988]. Theoretical model of block rotation along circular faults. *Tectonophysics*, *153*[1-4], 313-320.

Mørk, A., Dallmann, W., K., Djupvik, H., Johannessen, E. P., Larssen, G. B., Nagy, J., Nøttevedt, A., Olaussen, S., Pčelina, T. M., and Worsley, [1999]. Mesozoic lithostratigraphy., in: In W.K. Dallmann [ed.]: Lithostratigraphic Lexicon of Svalbard. Upper Palaeozoic to Quaternary Bedrock. Review and Recommendation for Nomenclature Use. Norwegian Polar Institute. Tromsø, pp. 127–214.

Morley, C. K., Nelson, R. A., Patton, T. L., and Munn, S. G. [1990]. Transfer zones in the East African rift system and their relevance to hydrocarbon exploration in rifts [1]. *AAPG Bulletin*, *74*[8], 1234-1253.

Mouslopoulou, V., Nicol, A., Little, T. A., and Walsh, J. J. [2007]. Displacement transfer between intersecting regional strike-slip and extensional fault systems. *Journal of Structural Geology*, *29*[1], 100-116.

Muraoka, H., and Kamata, H. [1983]. Displacement distribution along minor fault traces. *Journal of Structural Geology*, *5*[5], 483-495.

Nicol, A., Watterson, J., Walsh, J. J., and Childs, C. [1996]. The shapes, major axis orientations and displacement patterns of fault surfaces. *Journal of Structural Geology*, *18*[2-3], 235-248.

Nilsen K.T., B.C. Vendeville, J.-T. Johansen. 1995. Influence of regional tectonics on halokinesis in the Nordkapp Basin, Barents Sea AAPG Memoir

NPD. 2015. Fact pages - Norwegian Petroleum Directorate [NPD]. http://gis.npd.no/factmaps/html_21/

Nøttvedt, A., Cecchi, M., Gjelberg, J.G., Kristensen, S.E., Lønøy, A., Rasmussen, A., Rasmussen, E., Skott, P.H. and Van Veen, P.M., [1993]. Svalbard-Barents Sea correlation: a short review, in: T.O. Vorren, E.B. Ø.A. Dahl-Stamnes, E. Holter, B. Johansen, E. Lie and T.B. Lund [Ed.], Norwegian Petroleum Society Special Publications. Elsevier, pp. 363–375.

Omosanya, K. O., Johansen, S. E., and Harishidayat, D. [2015]. Evolution and character of supra-salt faults in the Easternmost Hammerfest Basin, SW Barents Sea. *Marine and Petroleum Geology*, *66*, 1013-1028.

Omosanya, K., O., and Alves, T. M. [2014]. Mass-transport deposits controlling fault propagation, reactivation and structural decoupling on continental margins [Espírito Santo Basin, SE Brazil]. *Tectonophysics*, *628*, 158-171.

Omosanya, K.O., Johansen, S.E., Abrahamson, P., [2016]. Magmatic activity during the breakup of Greenland-Eurasia and fluid-flow in Stappen High, SW Barents Sea. Mar. Pet. Geol. 76, 397–411. doi:10.1016/j.marpetgeo.2016.05.017

Peacock, D. C. P. [1991]. A comparison between the displacement geometries of veins and normal faults at Kilve, Somerset. *Proceedings of the Ussher Society*, *7*[4], 363-367.

Peacock, D. C. P., and Sanderson, D. J. [1991]. Displacements, segment linkage and relay ramps in normal fault zones. *Journal of Structural Geology*, *13*[6], 721-733.

Pochat, S., Castelltort, S., Choblet, G., and Van Den Driessche, J. [2009]. High-resolution record of tectonic and sedimentary processes in growth strata. *Marine and Petroleum Geology*, *26*[8], 1350-1364.

Ritzmann, O., and Faleide, J. I. [2007]. Caledonian basement of the western Barents Sea. *Tectonics*, *26*[5].

Safronova, P. A., Henriksen, S., Andreassen, K., Laberg, J. S., and Vorren, T. O. [2014]. Evolution of shelf-margin clinoforms and deep-water fans during the middle Eocene in the Sorvestsnaget Basin, southwest Barents Sea. *AAPG bulletin*, *98*[3], 515-544.

Schlische, R. W., Young, S. S., Ackermann, R. V., and Gupta, A. [1996]. Geometry and scaling relations of a population of very small rift-related normal faults. *Geology*, *24*[8], 683-686.

Schreurs, G. [2003]. Fault development and interaction in distributed strike-slip shear zones: an experimental approach. *Geological Society, London, Special Publications*, *210*[1], 35-52.

Schultz, R.A., [2000]. Fault-population statistics at the Valles Marineris Extensional Province, Mars: implications for segment linkage, crustal strains, and its geodynamical development. Tectonophysics 316, 169–193. doi:10.1016/S0040-1951[99]00228-0

Smelror, M., Petrov, O., Larssen, G.B. and Werner, S.C. [2009] ATLAS: geological history of the Barents Sea. Norges geologiske undersøkelse,Trondheim.

Soliva, R., and Benedicto, A. [2004]. A linkage criterion for segmented normal faults. *Journal of Structural Geology*, *26*[12], 2251-2267.

Spenser [1984]. The Petroleum Geology of the North European Margin, Proceeding of North European Margin Symposium [NEMS]. Trondheim. Springer

Sund, T., Skarpnes, O., Jensen, L.N. and Larsen, R.M., [1986]. Tectonic development and hydrocarbon potential offshore Troms, Northern Norway, Future Petroleum Provinces of the World. In: M.T. Halbouty, Editor, American Association of Petroleum Geologists Memoirs. 40, 615–627

Svånå, T.A., [2013]. Tectonic and Depositional Evolution of the Loppa High Area, Norwegian Barents Sea. AAPG Search and Discovery Article #90177©3P Arctic, Polar Petroleum Potential Conference & Exhibition, Stavanger, Norway, October 15-18, 2013.

Thorsen, C. E. [1963]. Age of growth faulting in southeast Louisiana.

Tvedt, A. B., Rotevatn, A., Jackson, C. A. L., Fossen, H., and Gawthorpe, R. L. [2013]. Growth of normal faults in multilayer sequences: a 3D seismic case study from the Egersund Basin, Norwegian North Sea. *Journal of Structural Geology*, *55*, 1-20.

Walsh, J. J., and Watterson, J. [1987]. Distributions of cumulative displacement and seismic slip on a single normal fault surface. *Journal of Structural Geology*, *9*[8], 1039-1046.

Walsh, J. J., and Watterson, J. [1988]. Analysis of the relationship between displacements and dimensions of faults. *Journal of Structural Geology*, *10*[3], 239-247.

Walsh, J. J., Watterson, J., Bailey, W. R., and Childs, C. [1999]. Fault relays, bends and branch-lines. *Journal of Structural Geology*, *21*[8], 1019-1026.

Walsh, J .J., Bailey, W. R., Childs, C., Nicol, A., Bonson, C. G. [2003]. Formation of segmented normal faults: a 3-D perspective. *Journal of Structural Geology*, 25, 1251–1262.

Whipp, P. S., Jackson, C., Gawthorpe, R. L., Dreyer, T., Quinn, D. [2014]. Normal fault array evolution above a reactivated rift fabric; a subsurface example from the northern Horda Platform, Norwegian North Sea. Basin Research, 26, 523-549.

Wilson, P., Elliott, G. M., Gawthorpe, R. L., Jackson, C. A. L., Michelsen, L., Sharp, I. R. [2013]. Geometry and segmentation of an evaporite-detached normal fault array: 3D seismic analysis of the southern Bremstein Fault Complex, offshore mid-Norway. Journal of Structural Geology, 51, pp. 74-91.

Worsley, D. [2008]. The post Caledonian development of Svalbard and the western Barents Sea. *Polar Research*, *27*[3], 298-317.

Xu, S., Nieto-Samaniego, A.F., Alaniz-Álvarez, S.A., Velasquillo-Martínez, L.G., Grajales-Nishimura, J.M., García-Hernández, J., Murillo-Muñetón, G., [2010]. Changes in fault length distributions due to fault linkage. J. Geodyn. 49, 24–30. doi:10.1016/j.jog.2009.08.002

Zampieri, D., and Massironi, M. [2007]. Evolution of a poly-deformed relay zone between fault segments in the eastern Southern Alps, Italy. *Geological Society, London, Special Publications*, *290*[1], 351-366.

Ze, T., Alves, T.M., [2017]. The role of gravitational collapse in controlling the evolution of crestal fault systems [Espírito Santo Basin, SE Brazil] – Reply. J. Struct. Geol. 98, 12–14. doi:10.1016/j.jsg.2017.03.005

Ziegler, W.H., Doery, R and Scott, J., [1986]. Tectonic Habitat of Norwegian Oil and Gas. In: A.M. Spencer et al., [Editors], Habitat of Hydrocarbons on the Norwegian Continental Margin. Norwegian Petroleum Society, Graham and Trotman, London, 339-354.

Øvrebø, O., and Talleraas, E. [1977]. The Structural geology of the Troms Area [Barents-Sea]. *GeoJournal*, *1*[1], 47-54.

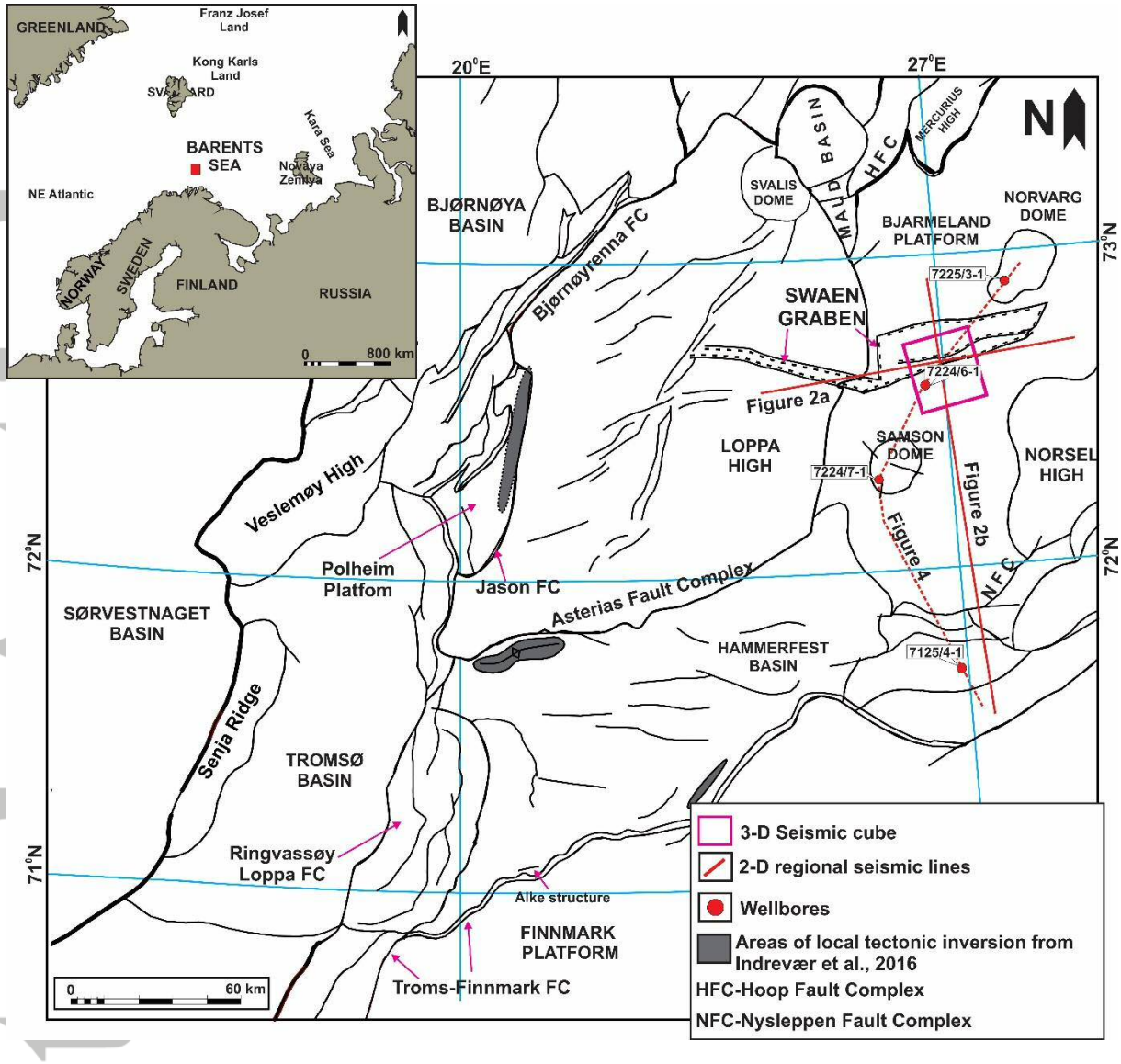

Figure 1: Structural map that shows the location of the study area, the seismic cube, and the regional 2-D seismic lines and wellbores that were used for the study in the context of other structural elements in the Southwestern Barents Sea. The study area is a component of the Swaen Graben and is located on the eastern flank of the Loppa High. *The inset shows the location of the Barents Sea in the context of Norway and surrounding countries. This map modified from Indrevær et al., [2016]. The dashed red line in the figure corresponds to the location of the correlation panel in Figure 4.*

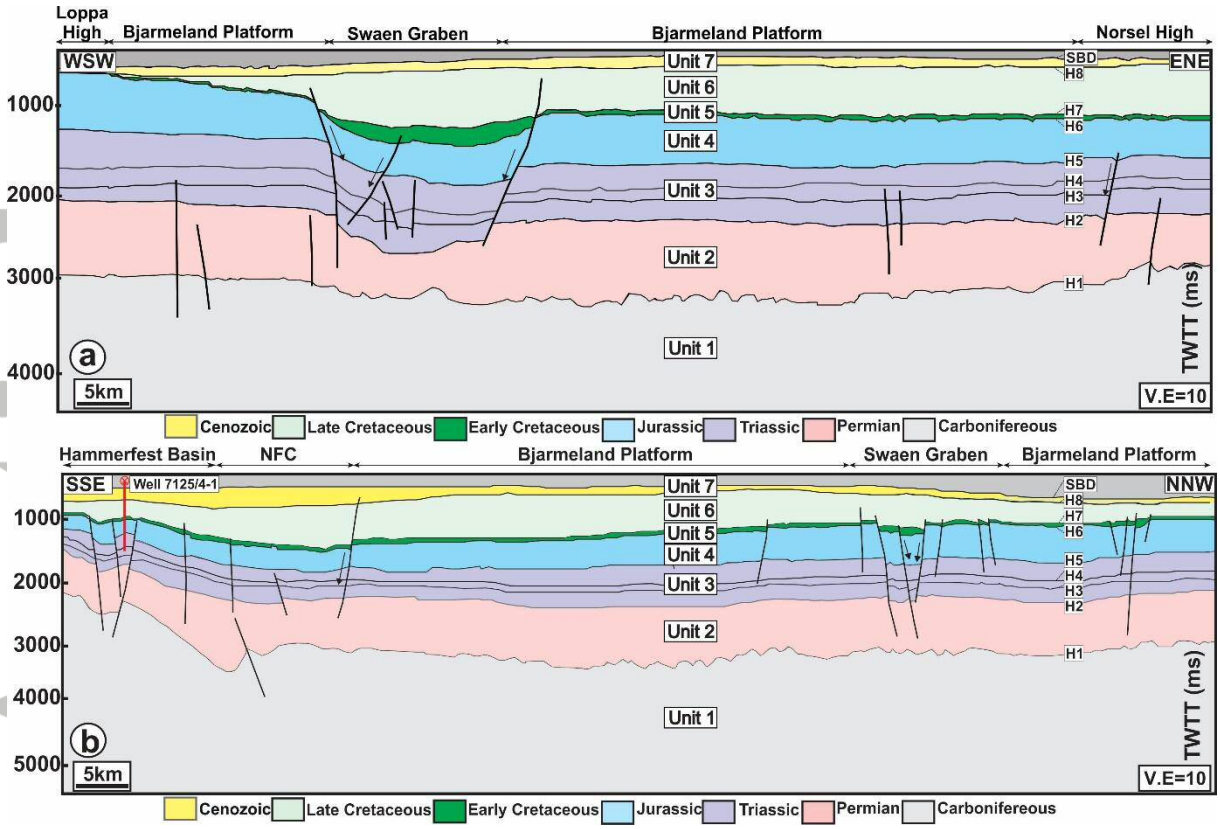

Figure 2: [a] Regional 2-D seismic section from the Norsel High to the eastern Loppa High, which shows the geology and tectonic framework of the study area in a regional context. The Swaen Graben shows evidence of intense extension with characteristic normal faults. [b] SSE to NNW regional 2-D seismic section from the Bjarmeland Platform to the Hammerfest Basin, which shows the geology and tectonic framework of the Swaen Graben in a regional context. *See Figure 1 for the locations of these sections.*

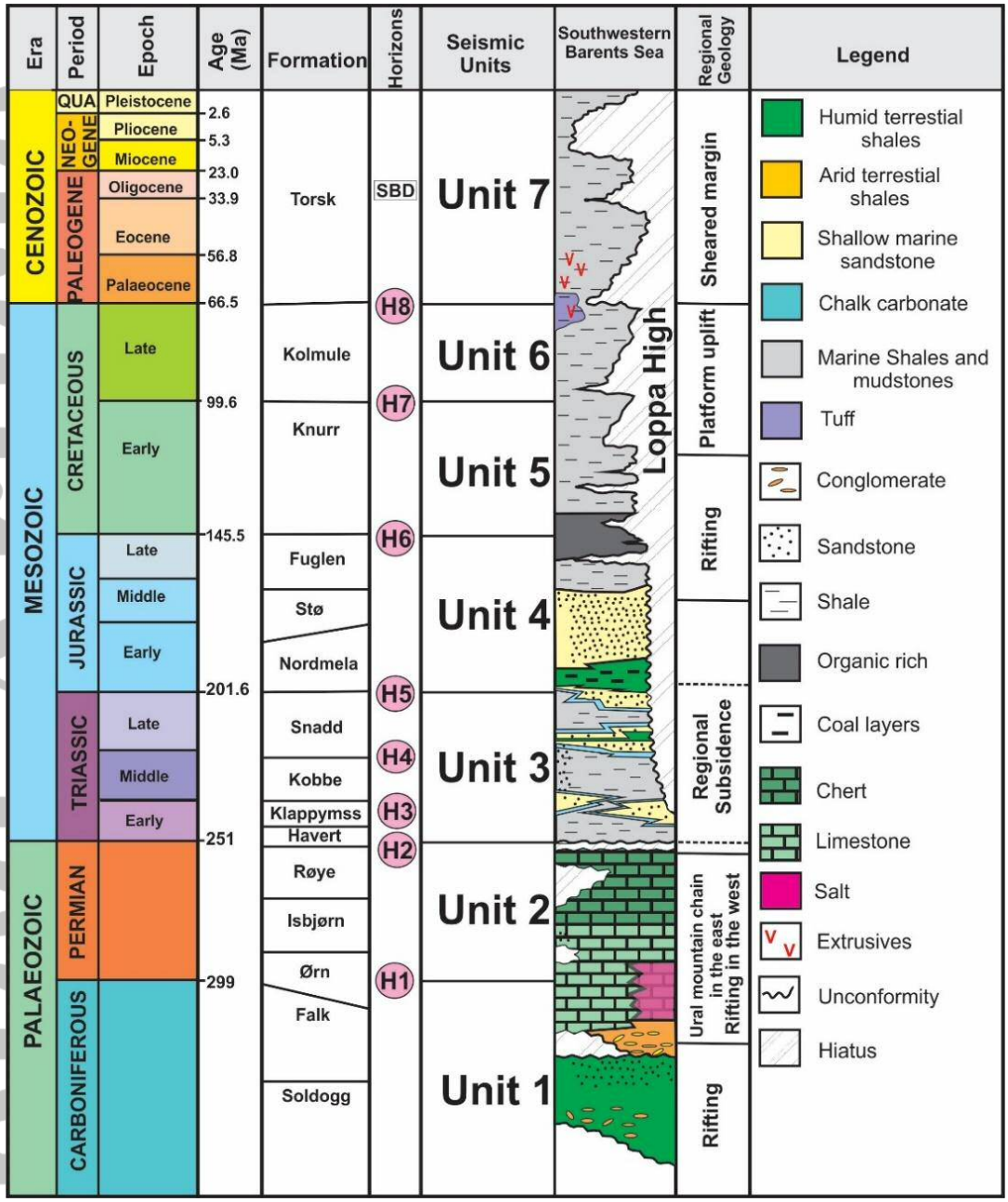

Figure 3: Summarized lithostratigraphic column of the Southwestern Barents Sea, which shows the ages, lithology and regional tectonic events that characterized the study area and surrounding basins from the Paleozoic to the present. The main horizons that were interpreted in this study were horizons H1 to H8. The formations of interest included the Carboniferous Ørn Formation to the Cretaceous Kolmule Formation. Based on Mattos et al. [2016] and Omosanya et al. [2015].

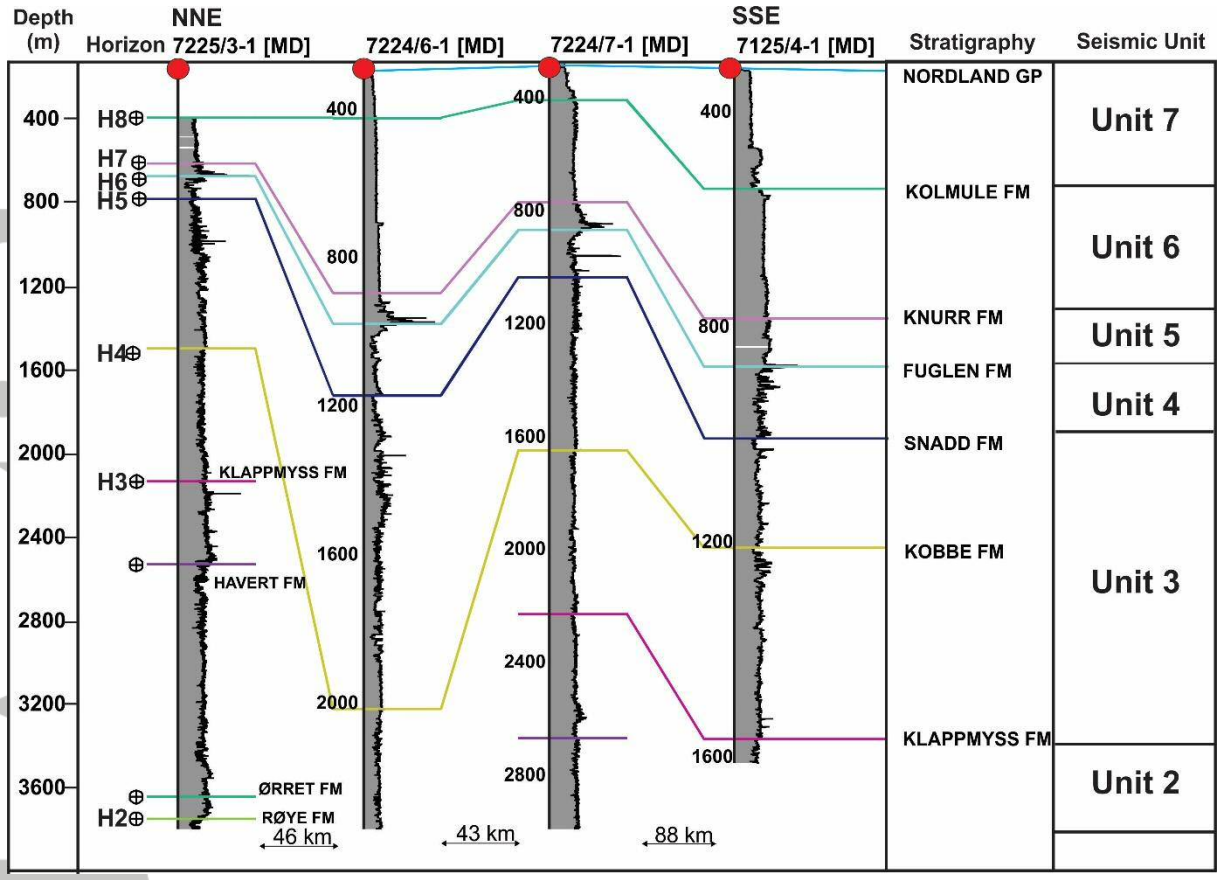

Figure 4: Regional chronostratigraphic correlation across the wellbores in Figure 1a. Wellbore 7224/6-1 was located in the Swaen Graben, while the other wellbores were used for regional correlations of the deeper horizons. *The wireline log in the figure is the gamma ray log.*

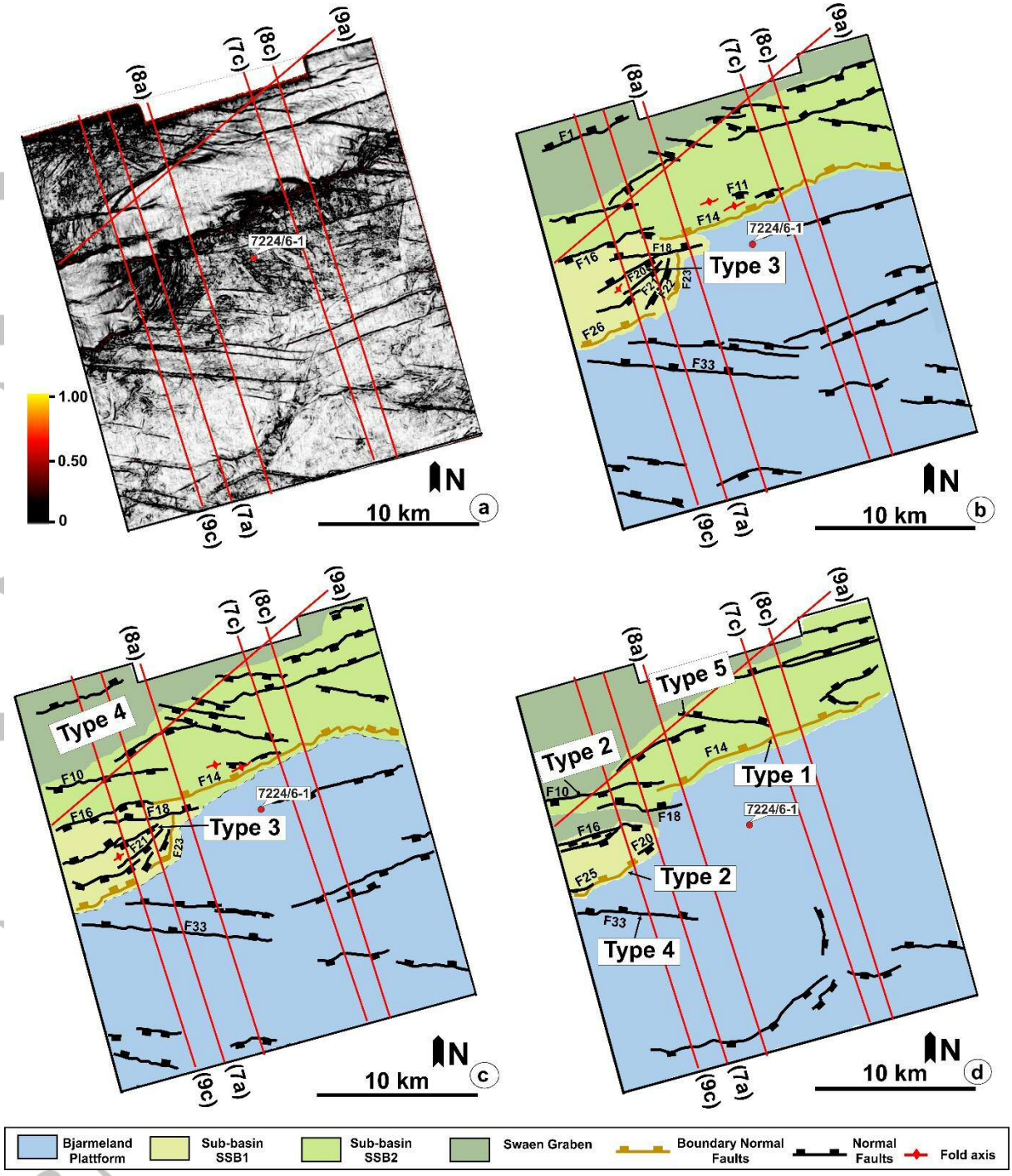

Figure 5: Structural maps across the Swaen Graben. [a] Variance time slice at a depth of 1100 ms TWTT that shows the faults that were interpreted in the study area. On the variance maps, faults are mapped as areas with low variance coefficients compared to the surrounding un-faulted units. [b] Structural map that highlights the faults that were interpreted from the slice in [a]. The maps shows that the faults that comprise the Swaen Graben divided the area into two sub-basins called Swaen Graben 1 and 2. [c]-[d] are structural maps at 1300 ms TWTT and 1900 ms TWTT depth, correspondingly.

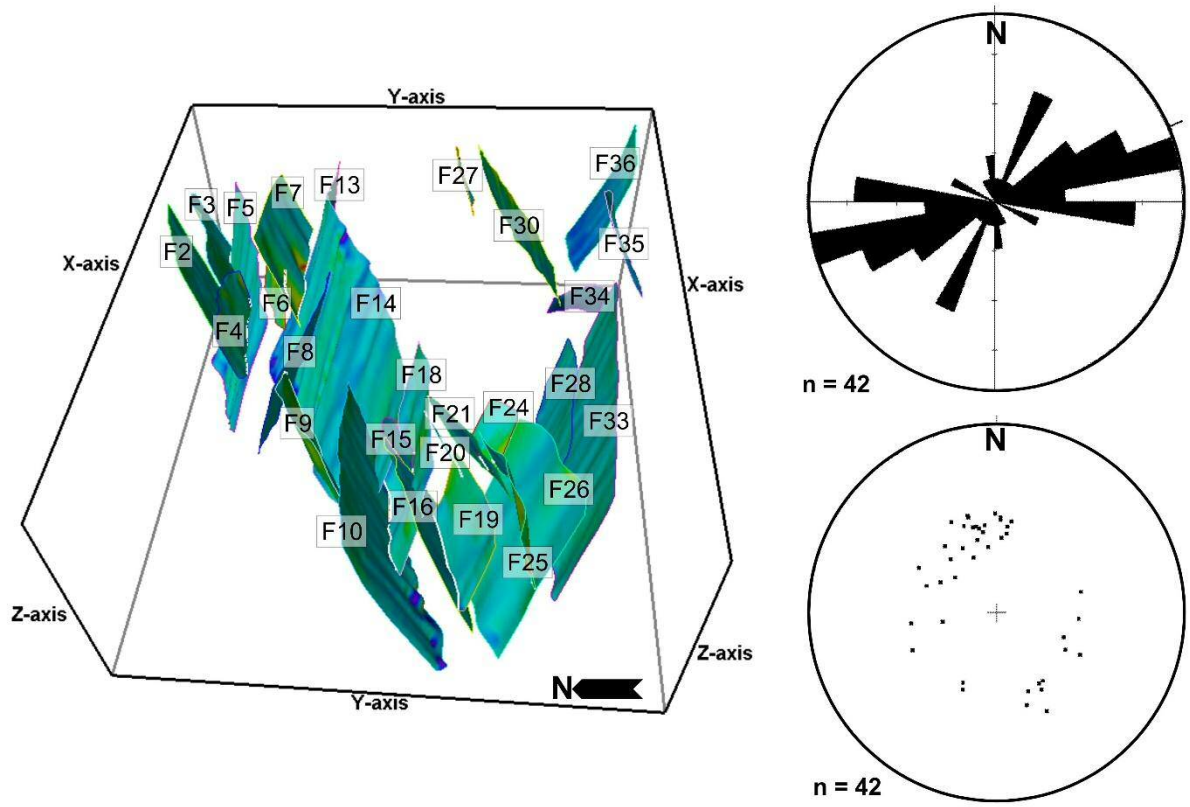

Figure 6:Three-dimensional view of the forty-two faults that were interpreted in this study. The vertical exaggeration is 5. Also shown in the figure are a rose diagram and a polar equal-area stereonet, which show the strike, dip direction and dip angle for all the faults. The dip angle for the faults varies from approximately 40^0 to < 90^0.

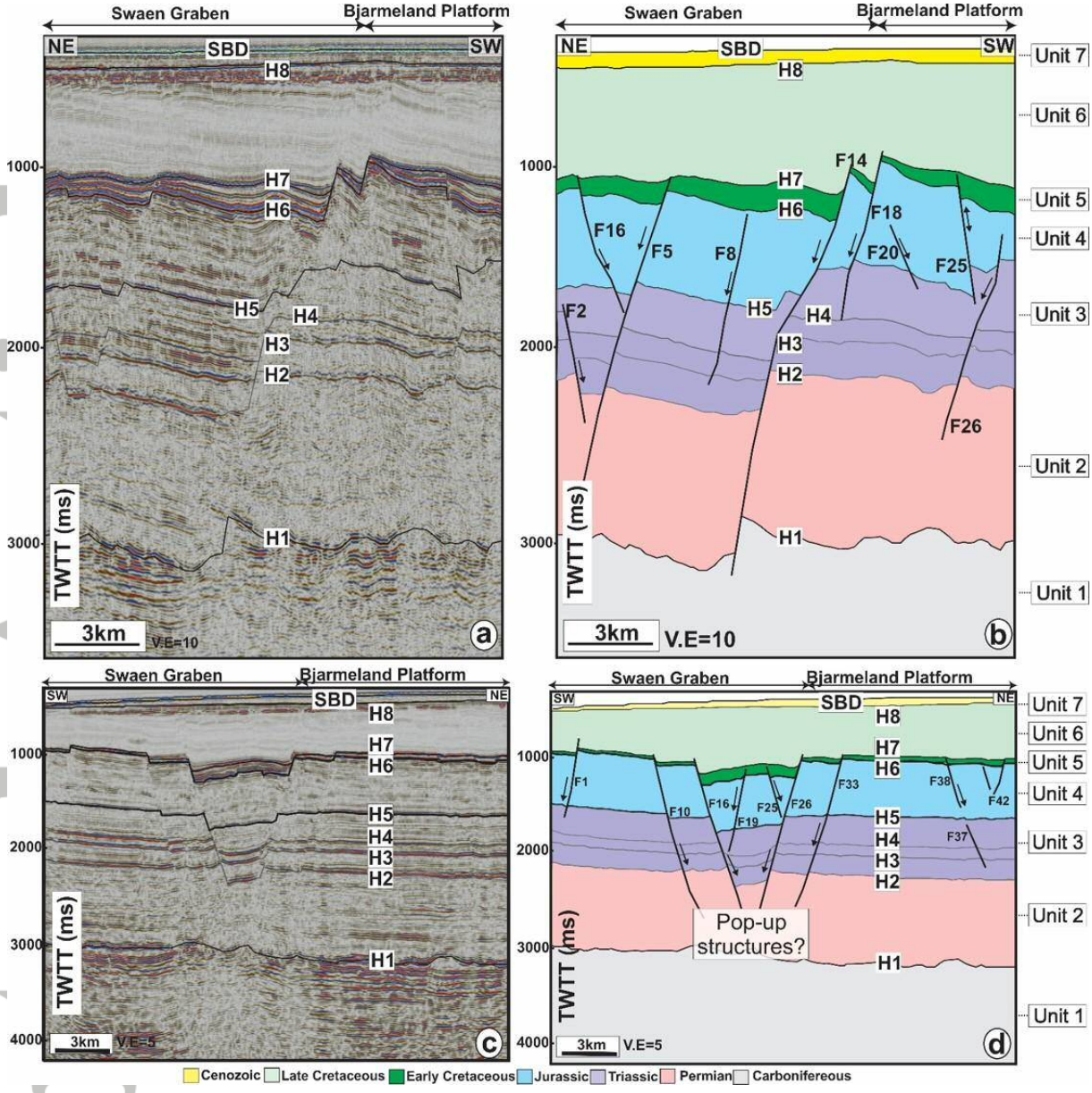

Figure 7: [a]-[b] Interpreted seismic section and corresponding line drawings that show examples of Type 1 faults [F5, F14 and F18]. Type 1 faults are laterally segmented and are the longest faults in the study area. [c]-[d] Interpreted seismic section and corresponding line drawings that show of Type 2 faults. These fault types were initially envisioned as pop-up structures delimited by F16 and F26 and that were related to strike-slip movement in the study area. Examples of such faults include F10, F16 and F26. *See Figure 5 for the locations of the seismic sections.*

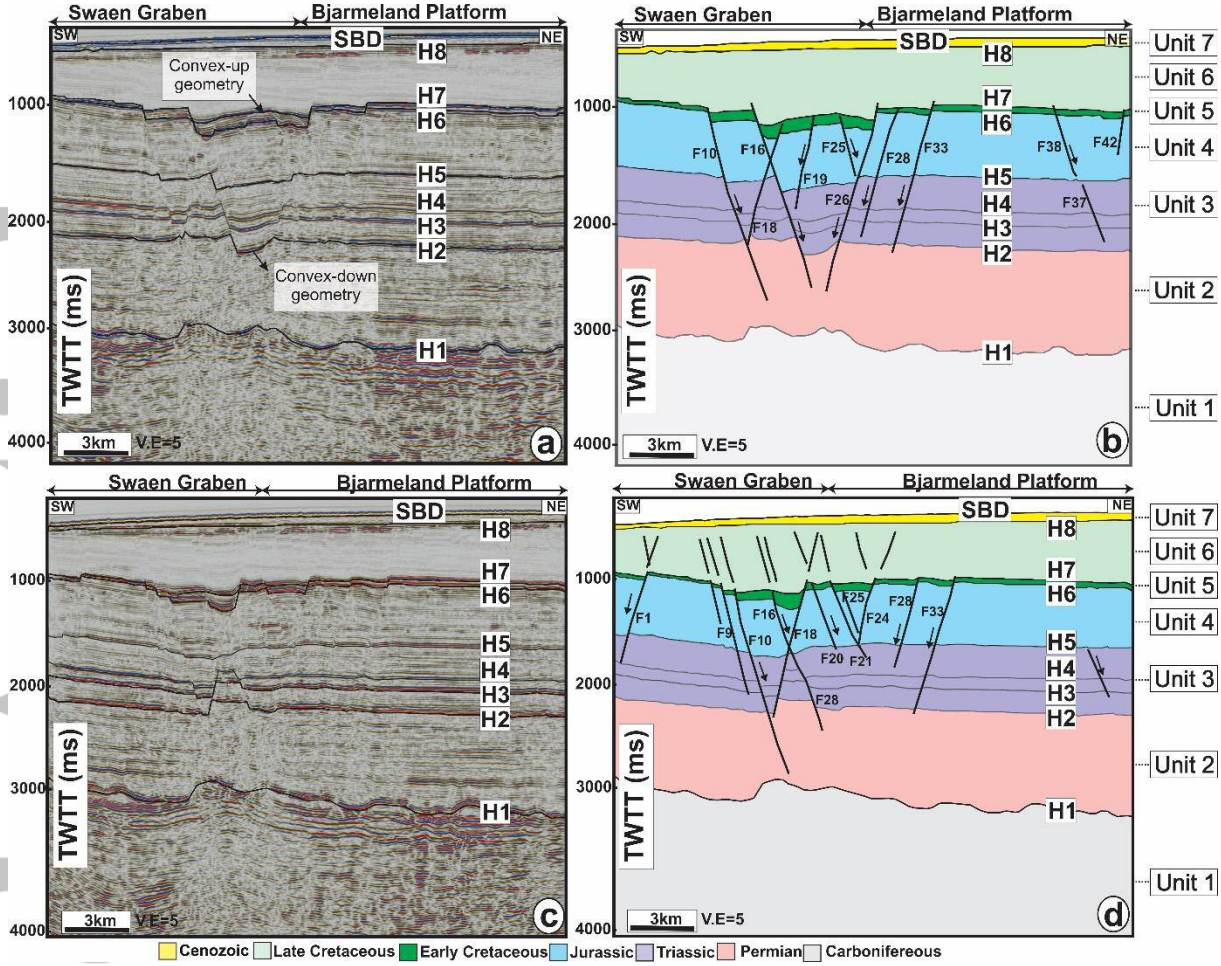

Figure 8: [a]-[b] Additional interpreted seismic section and corresponding line drawings that show examples of Type 2 faults, such as F10, F16 and F26. Also shown is the convex-up geometry of the Early Cretaceous strata across the faults. Here, the H6-H7 strata are uplifted relative to the underlying H2-H6 strata [c]-[d]: Interpreted seismic section and corresponding line drawings that show examples of Type 3 faults [e.g., F20 and F21]. The Type 3 faults are synthetic faults with general NE dips. In map view, these faults have similar geometry to Riedel shears or transfer faults and are common along the boundary of F18. *See Figure 5 for the locations of the seismic sections.*

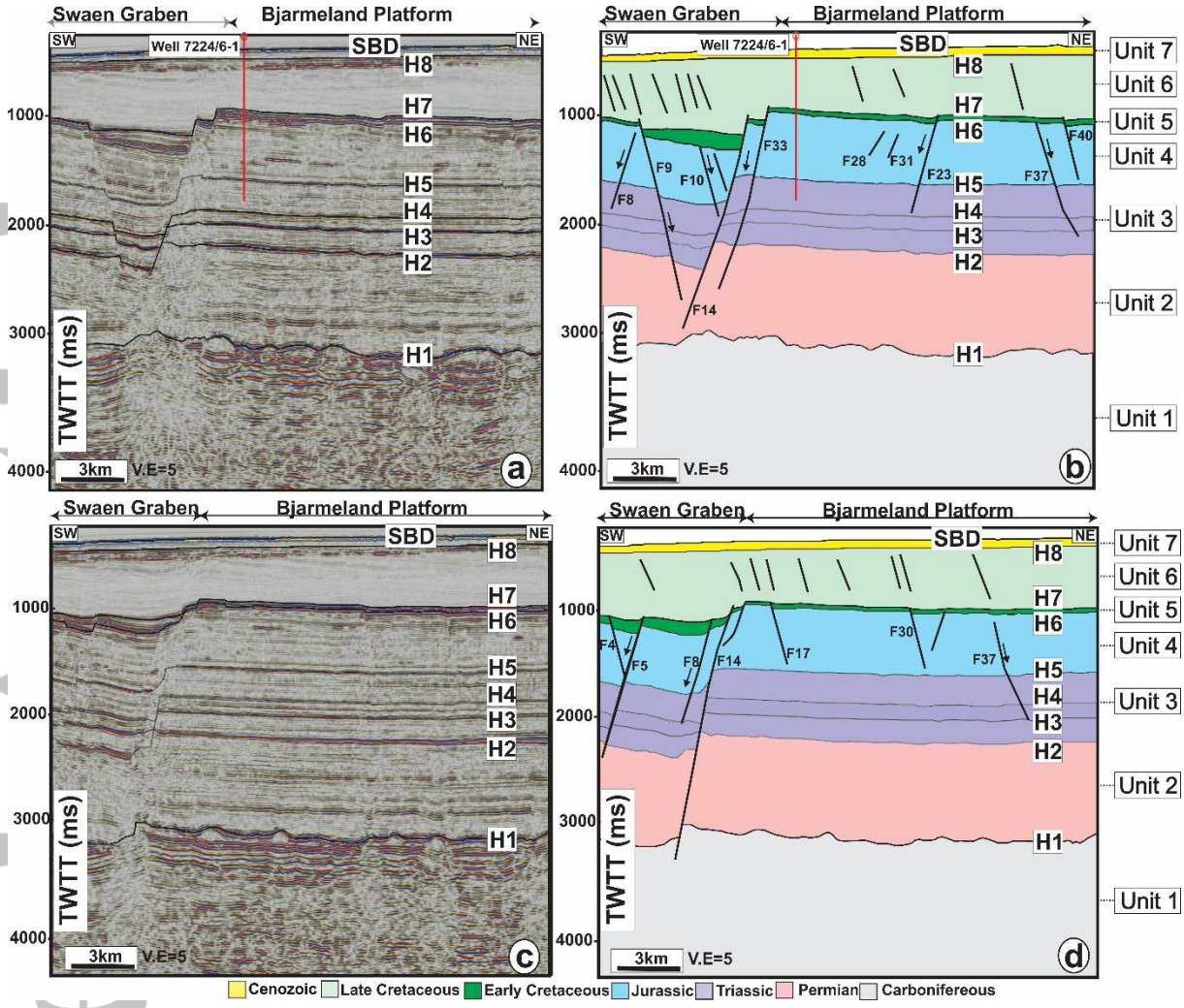

Figure 9: [a]-[b] Interpreted seismic section and corresponding line drawings that show examples of Type 4 faults [e.g., F33 and F37]. The Type 4 faults had their upper sections abruptly terminated beneath horizon H7 and were considered to be isolated and kinematically decoupled faults. This fault decoupling was proposed to be related to Cretaceous erosion. [c]-[d] Additional interpreted seismic section and corresponding line drawings that show examples of Type 4 faults [F35 and F37] and how they were decoupled stratigraphically below the Early Cretaceous interval. Minor faults within the Late Cretaceous units provide evidence for disparate timing and mechanism of the faulting in the study area. *See Figure 5 for the locations of the seismic sections.*

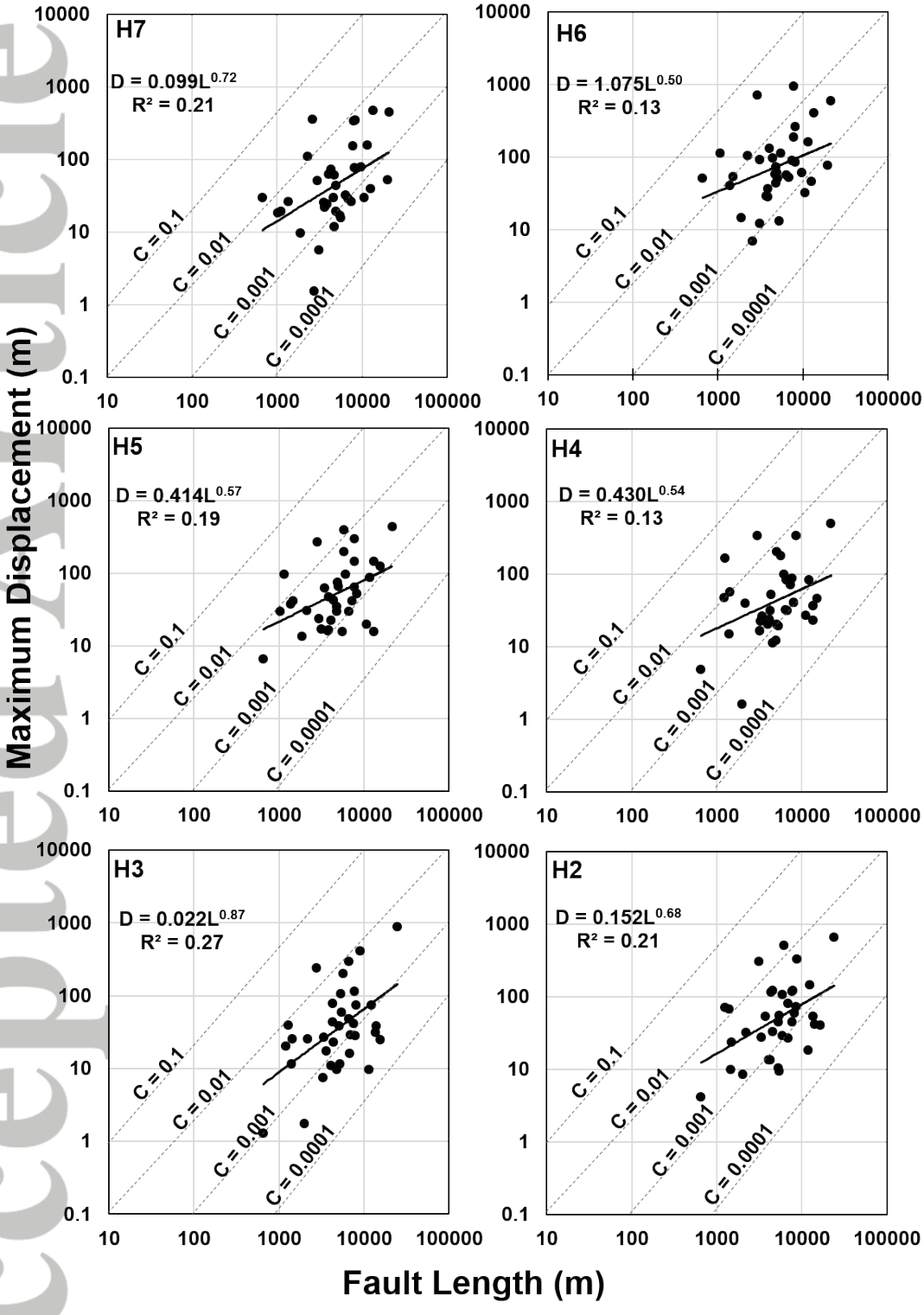

Figure 10: Maximum displacement [D_{max}] versus length [L] plots for all forty –two faults across horizons H2 to H7. The majority of the faults show a D:L ratio between 1:100 and 1:1000.

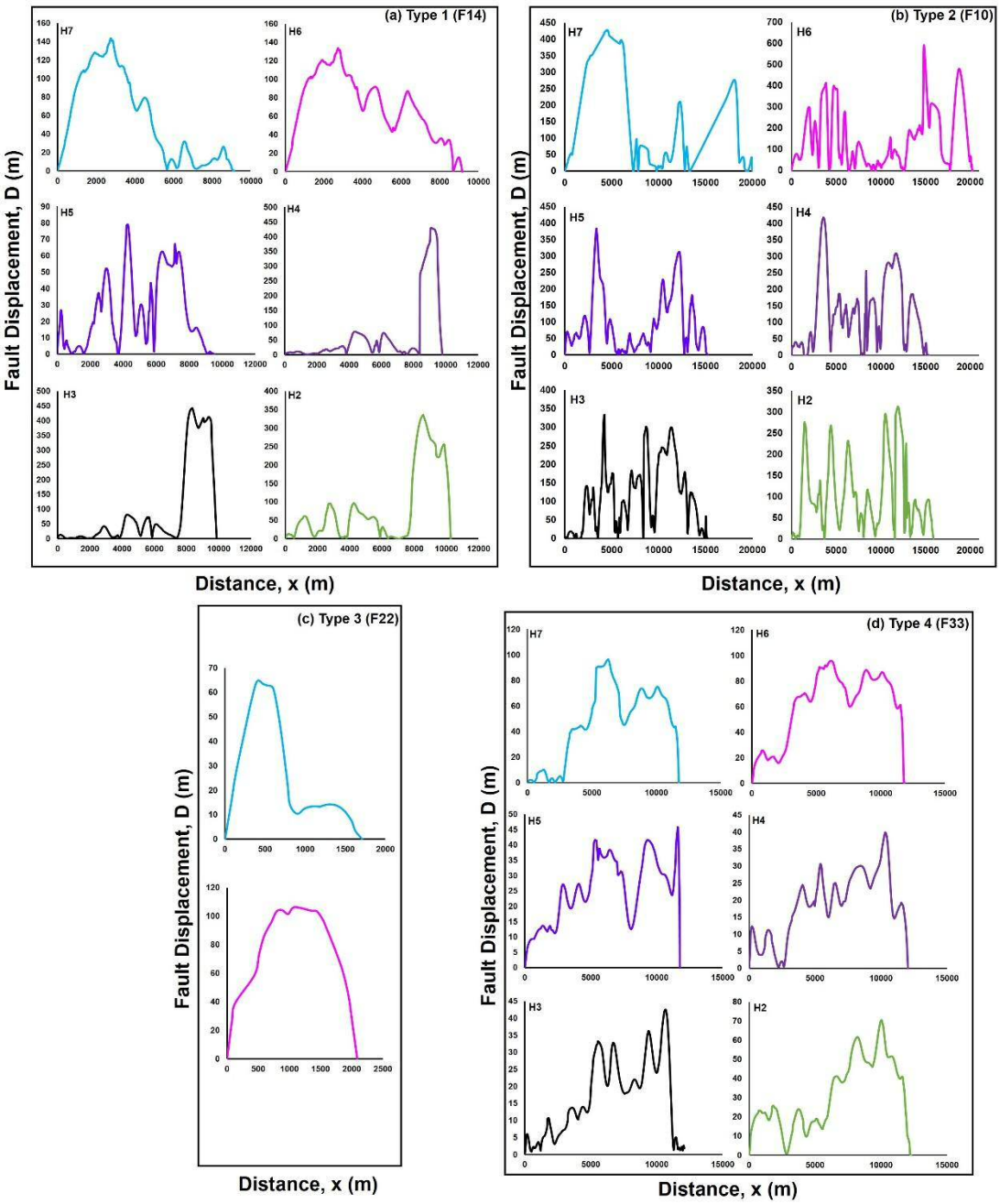

Figure 11: Fault-displacement [D] versus distance [x] plots for the [a] Type 1 [b] Type 2 [c] Type 3 and [d] Type 4 faults in the Swaen Graben. The D-x plots include c-skewed, c-type and skewed M-type profiles. In addition, the plots show that the faults have multiple segments, which is evidence for their complex lateral segmentation. The skewness of the profiles probably evidences their complex evolution and segmentation. For example, the Type 1 faults have different skewness direction from H2 to H7.

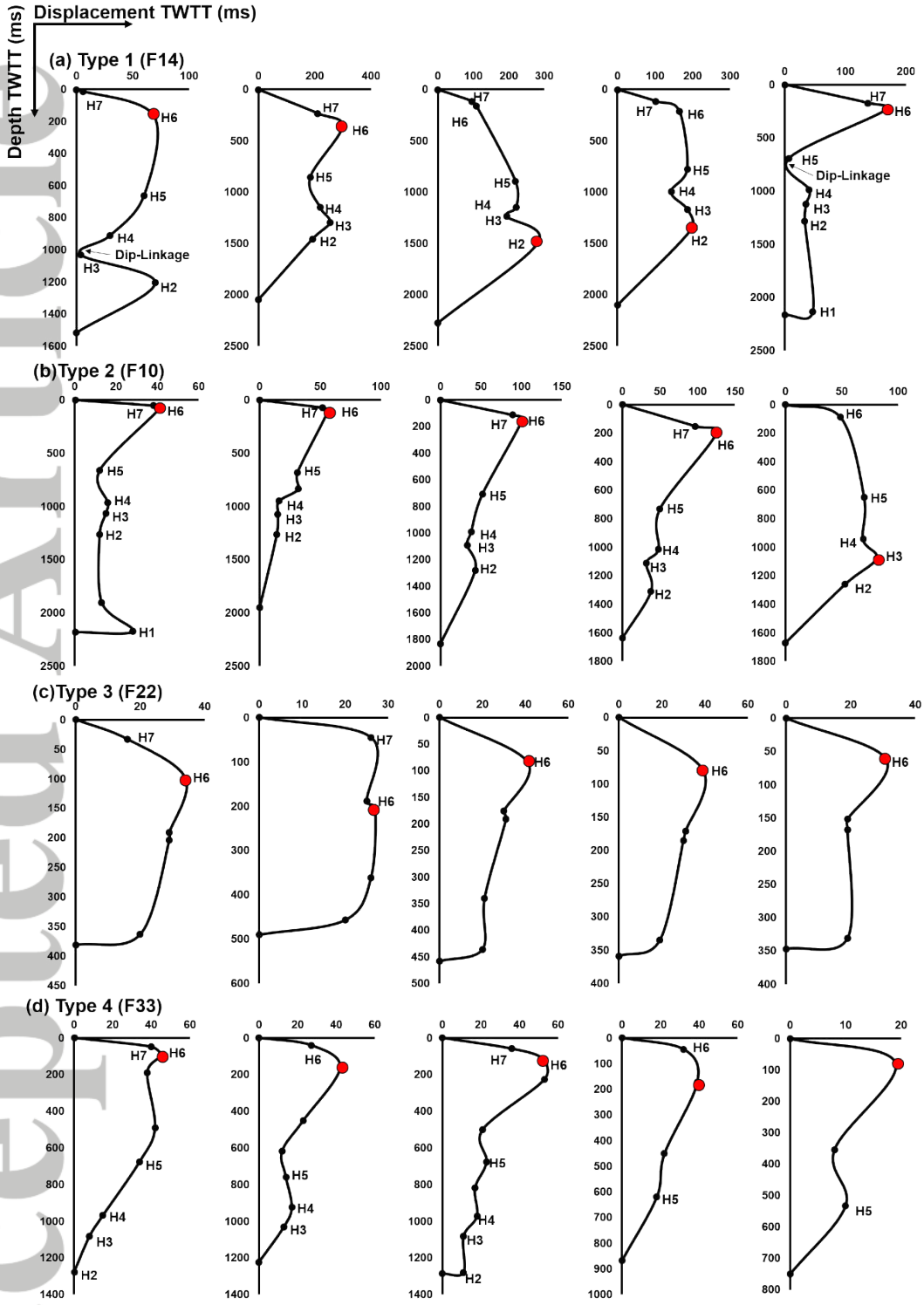

Figure 12: Displacement [D] versus depth plots for all four fault types. The plots include hydrid types [Type 1], C-type and skewed C-type [Type 2], M-type [Type 3] and skewed C-types profiles. The points of maximum displacement-d_{max} are marked with red circles.

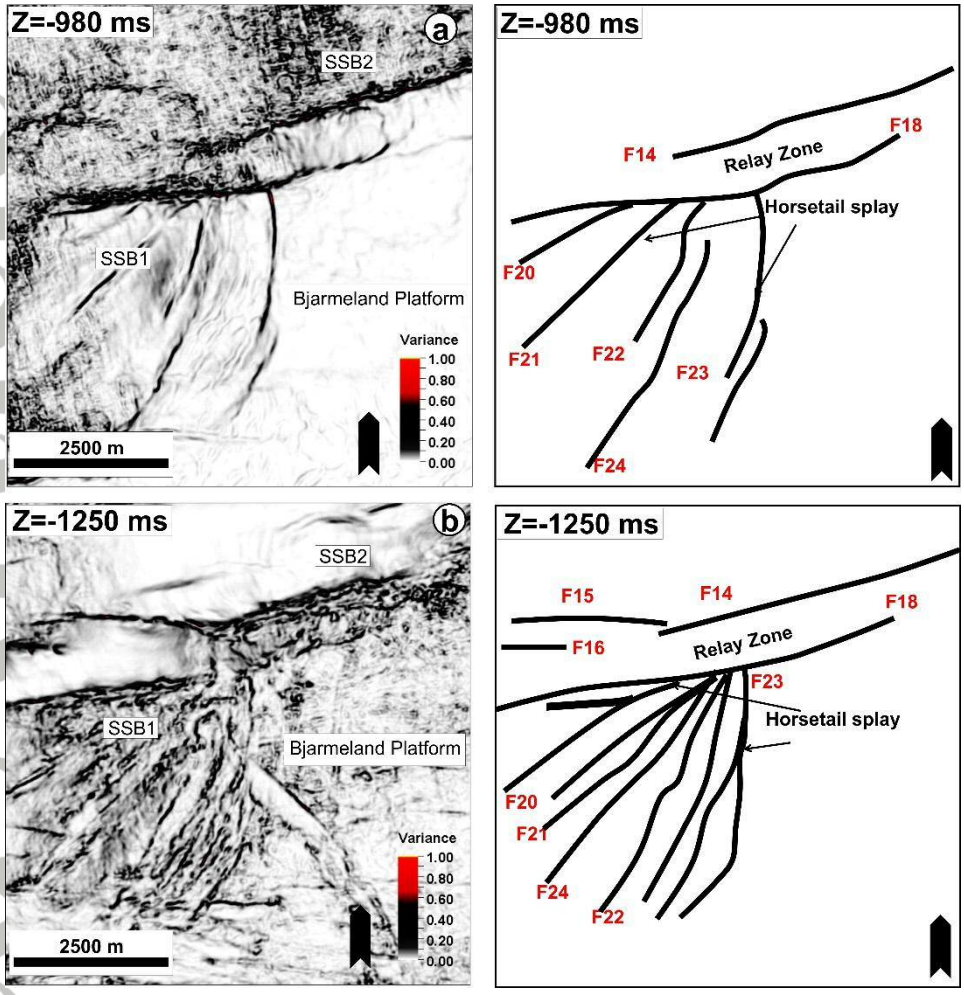

Figure 13: [a]-[d] Variance time slices from 980 ms to 1500 ms TWTT, which show the outline of the horsetail splay faults [F19-F24] that are associated with fault F18. Also shown in the figure is the relay zone between F14 and F18, which connects sub-basins SSB1 and SSB2.

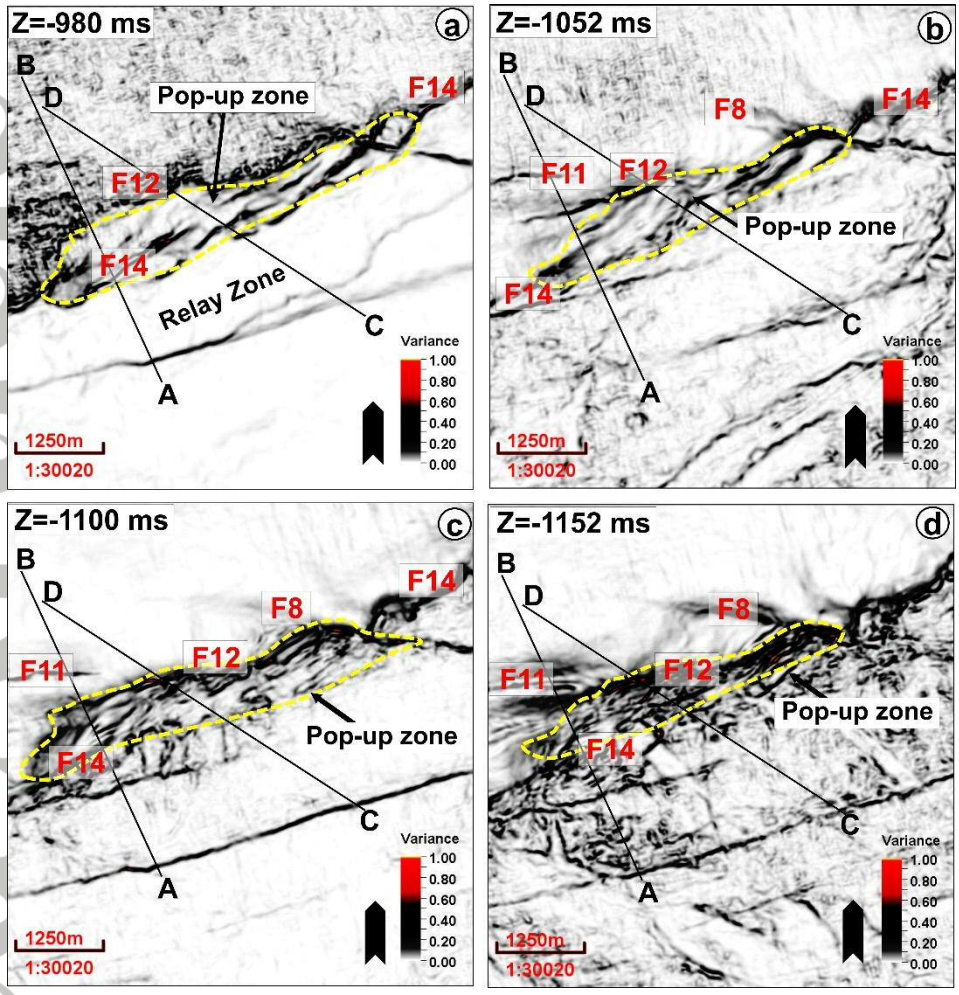

Figure 14: [a]-[d] Map that show the variation in the architecture of the pop-up structures along the western flank of F14. Several small-scale faults are associated with the pop-up structure. Traverse AB and CD correspond to the locations of the seismic sections in Figure 15.

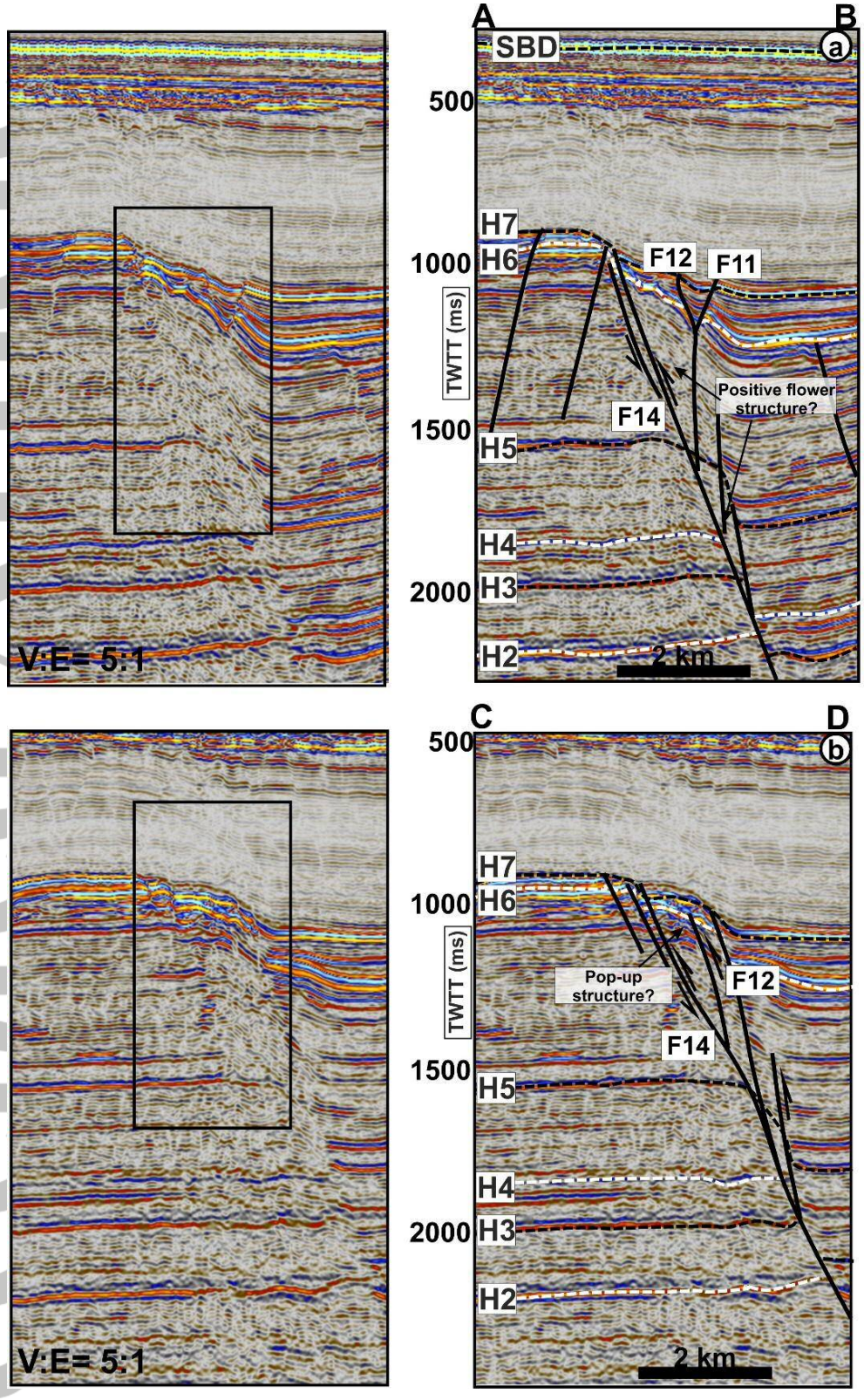

Figure 15: [a]-[b] Uninterpreted and interpreted arbitrary lines through the pop-up structure in Figures 13 and 15. On the seismic section, the structure is revealed uplifted blocks on the footwall of F14 and is interpreted as a positive flower structure in this work. An alternative interpretation is considered to include mild inversion of normal faults in response to the left-lateral movement along F18. *See Figure 14c for the locations of the seismic sections.*

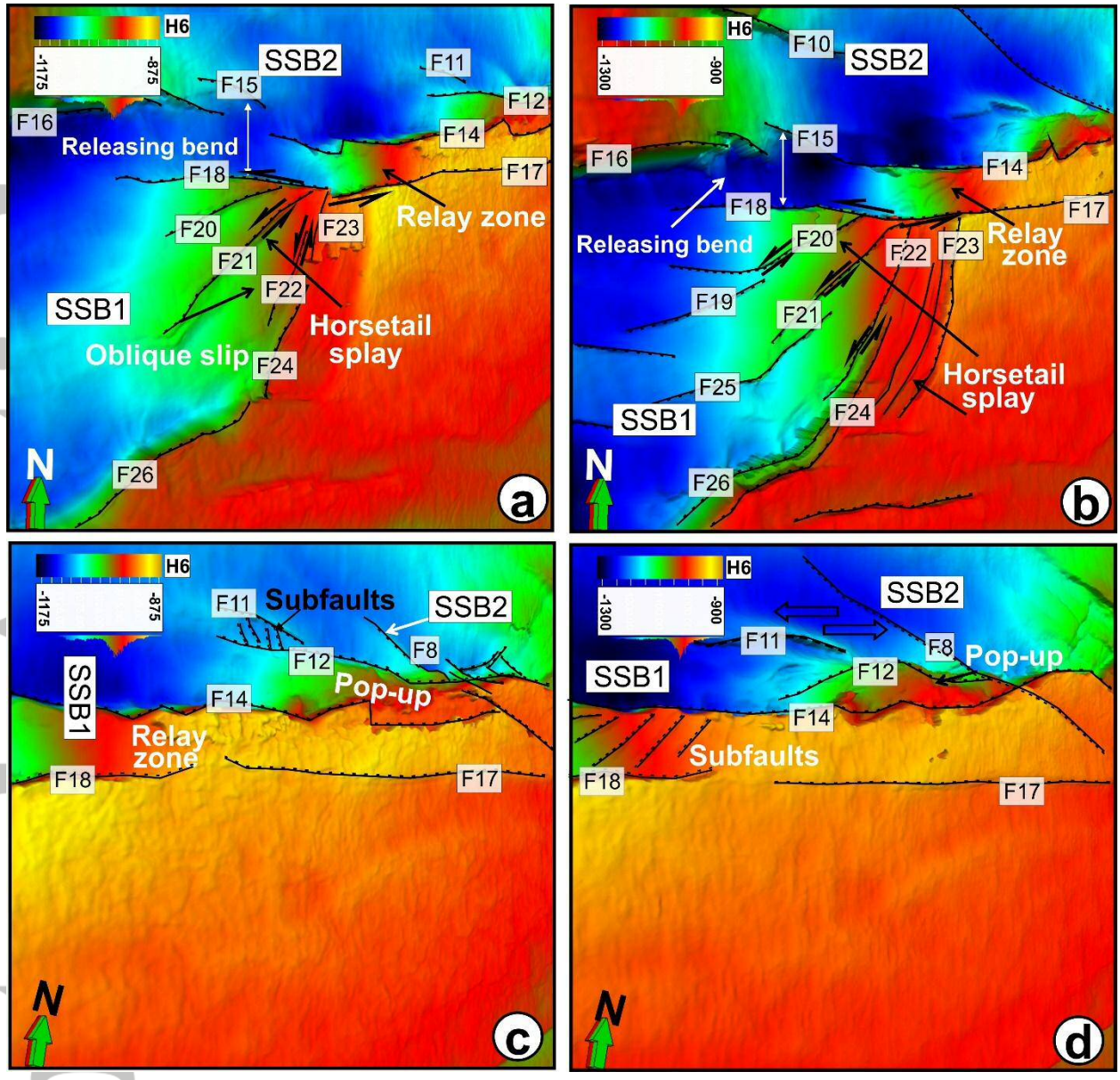

Figure 16: Geometrical evidence for strike-slip movement in the Swaen Graben, which include the presence of an interpreted pop-up structures, releasing bend, horsetail splay faults, relay zone and stepovers. The pop-up structure in Figure 15 is attributed to the contraction of the faults blocks at F14 in response to sinistral movement along F18. The map is a 3-D view of the structural map for Horizon H6. The sub-faults are transfer faults that link the faults at the relay zone.

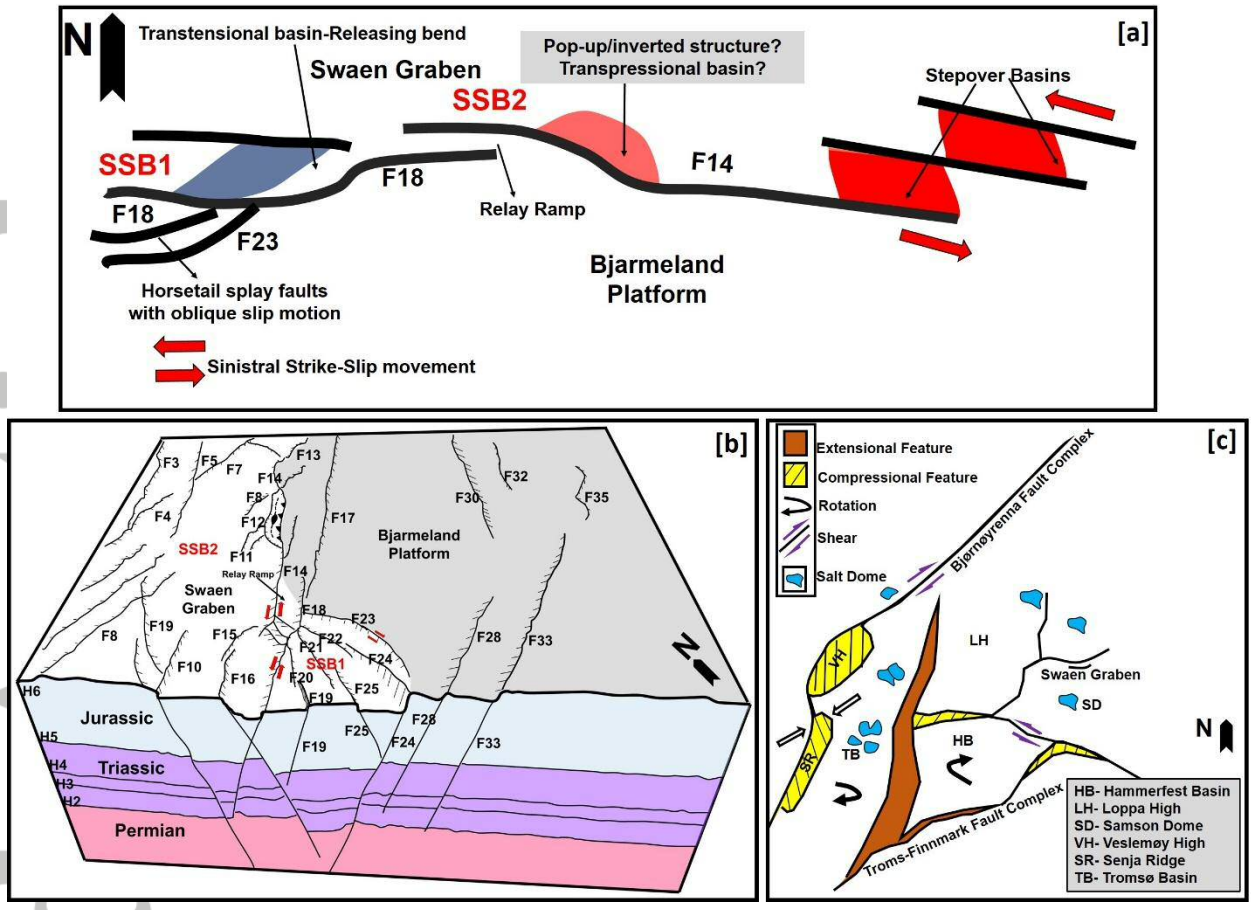

Figure 17: [a] Conceptual diagram that show the different fault types in the study area and the evidence for strike-slip movement in the Swaen Graben. F14 is a strike-slip fault that formed probably at a restraining bend, which resulted in the formation of the associated flower structure. F18 is a strike-slip faults that is characterised by extensional horsetail splay faults at its tip. Both faults are linked by transfer faults at the relay zone. [b] 3-D view of the interpreted fault types in the Swaen Graben. The vertical exaggeration is 5. [c] Regional stress regime and tectonic activities prevalent during the Late Jurassic to Early Cenozoic [Modified after Gabrielsen and Færseth, 1988].